Available online at www.sciencedirect.com
ScienceDirect
Tectonophysics 428 (2006) 1–31
TECTONOPHYSICS
www.elsevier.com/locate/tecto

Mechanisms and duration of non-tectonically assisted magma emplacement in the upper crust: The Black Mesa pluton, Henry Mountains, Utah

Michel de Saint-Blanquat [a,*], Guillaume Habert [a], Eric Horsman [b], Sven S. Morgan [c], Basil Tikoff [b], Patrick Launeau [d], Gérard Gleizes [a]

[a] CNRS — LMTG/Observatoire Midi-Pyrénées, Université Paul-Sabatier, 14 av. Edouard-Belin, 31400 Toulouse, France
[b] Department of Geology and Geophysics, University of Wisconsin-Madison, Madison, Wisconsin 53706, USA
[c] Department of Geology, Central Michigan University, Mount Pleasant, Michigan 48859, USA
[d] Laboratoire de Pétrologie Structurale, Université de Nantes, 2 rue de la Houssinière BP 92208, 44322 Nantes cedex 3, France

Received 17 August 2005; received in revised form 9 July 2006; accepted 13 July 2006

Abstract

A new study of Black Mesa pluton (Henry Mountains, Colorado Plateau, Utah, USA) indicates that it is a classic example of a small upper-crustal pluton assembled over a few years by incremental amalgamation of discrete magma pulses. The results of our petrostructural study of the pluton interior allow us to constrain the geometry, kinematics and timing of the processes. The symmetric internal fabric is interpreted as an evidence for a feeding by below and not laterally. The observed rotation of the lineation, from WNW–ESE on the very top to NNE–SSW below, lead us to propose that the fabric at the base of the pluton is a record of magma infilling process, and the fabric at the very top is a record of the strain due to the relative movement between magma and wallrocks. A consequence is that except at the contact between pluton and wallrocks (top and margins), the stretching direction, recorded by the lineation, is not parallel to the flow direction of the magma i.e. displacement. The Black Mesa pluton is a sheeted laccolith on its western edge and a bysmalith on its eastern edge. This E–W asymmetry in pluton geometry/construction and the symmetrical internal fabric indicates that the apparently different west and east growth histories could have occurred simultaneously. Our field data indicate pluton growth through an asymmetric vertical stacking of sill-like horizontal magma sheets.

One-dimensional thermal models of the pluton provide maximum limits on the duration of its growth. We have constrained the number, the thickness, and the frequency of magma pulses with our structural observations, including: (1) the emplacement of the pluton by under-accretion of successive magma pulses, (2) the absence of solid-state deformation textures at internal contacts, and (3) the apparent absence of significant recrystallization in the wallrocks. Our results suggest that the emplacement of the Black Mesa pluton was an extremely rapid event, with a maximum duration on the order of 100 years, which requires a minimum vertical displacement rate of the wallrocks immediately above the pluton greater than 2 m/yr. Finally, our data show that the rates of plutonic and volcanic processes could be similar, a significant result for interpretation of magma transfer in arc systems.

Keywords: Pluton; Rates; Magma; Laccolith; Bysmalith; Henry Mountains

* Corresponding author.
E-mail address: michel@lmtg.obs-mip.fr (M. de Saint-Blanquat).

0040-1951/$ - see front matter © 2006 Elsevier B.V. All rights reserved.
doi:10.1016/j.tecto.2006.07.014

1. Introduction

One of the most important questions about magmatic processes in arcs is how plutons are constructed, in terms of mechanism, duration, and rate. Recent studies have questioned the image of plutons as "big-tank" magma chambers, and emphasized incremental pluton construction by amalgamation of small magma pulses (e.g. Glazner et al., 2004). Other studies have demonstrated the role of horizontal and/or vertical translation of country rocks as the major space-making mechanism for magma emplacement in both the upper crust (Cruden, 1998; Tikoff et al., 1999; Acocella, 2000; Cruden and Mc Caffrey, 2001; Habert and Saint-Blanquat, 2004), and in the middle crust (Morgan et al., 1998; Saint-Blanquat et al., 2001). Until at least a depth of 15 km, and perhaps deeper, magma emplacement is mainly accommodated by roof lifting, itself accommodated by an upward displacement of Earth's surface. Estimates of the rate and duration of all these magmatic and associated "wallrocks" processes have rarely been published (Minakami et al., 1951; Corry, 1988; Webber et al., 1999; Saint-Blanquat et al., 2001; Coulson et al., 2002; Habert and Saint-Blanquat, 2004), but are of prime importance in order to get data about the timescale of magmatic processes and mass transfer in the lithosphere. One difficulty in studying these processes is that the emplacement of magmatic rocks at a depth results from a combination of internal magmatic processes (magmatic pressure or influx rate) and external tectonic processes (regional deformation) (Hutton, 1988). The internal structure, or fabric, of the pluton is the record of the combination of these processes (Saint-Blanquat et al., 1998; Barros et al., 2001, Neves et al., 2003), making structural patterns in plutons difficult to interpret in terms of magmatic versus tectonic processes alone. The Tertiary dioritic intrusions of the Henry Mountains (Utah) constitute an exceptional natural example where internal structures can be unambiguously interpreted in terms of purely magmatic processes. The Henry Mountains are located in the Colorado Plateau, which experienced no significant regional deformation during or since magma emplacement. The country rocks are consequently horizontal and undeformed, and constitute ideal markers that allow us to quantify the strain path (translation, rotation, strain) associated with forceful emplacement of magma, without any interference with tectonics. Moreover, the intrusions are compositionally homogeneous and contain an aphanitic groundmass. This suggests rapid cooling which rules out any post-intrusive overprinting of the magmatic fabric. Finally, the combination of a strong magmatically-induced vertical uplift and differential erosion between sedimentary and magmatic rocks has exposed the 3D shape of the plutons and made observation of both base and top contacts possible.

The aim of this paper is to constrain the mechanism and the duration of the emplacement of the Black Mesa pluton (BMp), one of the satellite intrusions of the Mt Hillers intrusive complex, Henry Mountains, Utah. We have combined structural, rock magnetic, and petrological studies of the intrusion with a numerical simulation of the evolution of temperature during a non-instantaneous multi-pulse emplacement. Our results regarding the internal structure of the pluton are in general agreement with the emplacement model of Pollard and Johnson (1973), mainly based on wallrock geometry, but allow us to precisely constrain the geometry, kinematics and timing of the processes. We find in particular that the BMp cannot be strictly defined as a laccolith or a bysmalith, either in terms of final shape or growth mechanisms. Rather, it is a hybrid between a punched and a sheeted laccolith, following the Corry (1988) terminology, although the word "laccolith" is not appropriate. As the use of this classic terminology could lead to semantic problems with words having both a descriptive (pluton shape) and an interpretative (pluton construction) sense, we refer to the Black Mesa *pluton* instead of bysmalith or laccolith. We find an asymmetry in pluton geometry and construction as the west side is thinnest and was constructed by bending, rotation and faulting of wallrocks without loss of continuity between adjacent blocks, whereas the east side of the pluton is thickest and was constructed by fault lifting of the roof with a 200 m high vertical fault scarp. We also find a symmetrical internal fabric within the pluton, which shows that the different west and east growth histories could have occurred simultaneously. Consequently, the fault stage (i.e. the "bysmalith" stage) is not necessarily the record of an increase of the infilling rate, as previously suggested, but could be simply the expression of a greater volume of magma intruded in the eastern part of the pluton. Our data are then more in agreement with a general pluton growth through asymmetric vertical stacking of sill-like horizontal magma sheets, and our numerical simulations suggest that a minimum roof uplift rate on the order of 2 m/yr was necessary for the emplacement of the body in order to produce the observed internal texture.

2. The Henry Mountains

The Henry Mountains, in south-eastern Utah, are about 60 km long and trend roughly North–South

(Fig. 1). They are constituted by five main peaks composed of sedimentary domes with igneous cores, from north to south Mt Ellen, Mt Pennell, Mt Hillers, Mt Holmes and Mt Ellsworth, which are surrounded by numerous dikes, sills and minor laccoliths. Intrusions are situated on the gently dipping (1–2° West) eastern limb of a North–South trending basin, that is bounded on the west by an east-vergent monocline known as the Waterpocket Fold (Hunt et al., 1953). The intrusive rocks are microgranular porphyritic diorites and quartz diorite porphyries (Engel, 1959) emplaced into Permian to Mesozoic sandstone and shale dominated formations. $^{40}Ar/^{39}Ar$ and fission-track dating on the intrusive rocks of the Henry Mountains yields middle to late Oligocene ages (23–31 Ma) for the five main intrusion centres, with an age of 29.35 ± 0.33 Ma for Mt Hillers and its satellite intrusions (Suvillan et al., 1991; Nelson et al., 1992; Nelson, 1997).

Magmatism of the Henry Mountains and other laccoliths of the Colorado Plateau, such as those found in the La Sal and Abajo Mountains, was contemporaneous with voluminous magmatism of the San Juan and Reno–Marysvale volcanic fields outside the plateau region (Armstrong and Ward, 1991). Thus, although

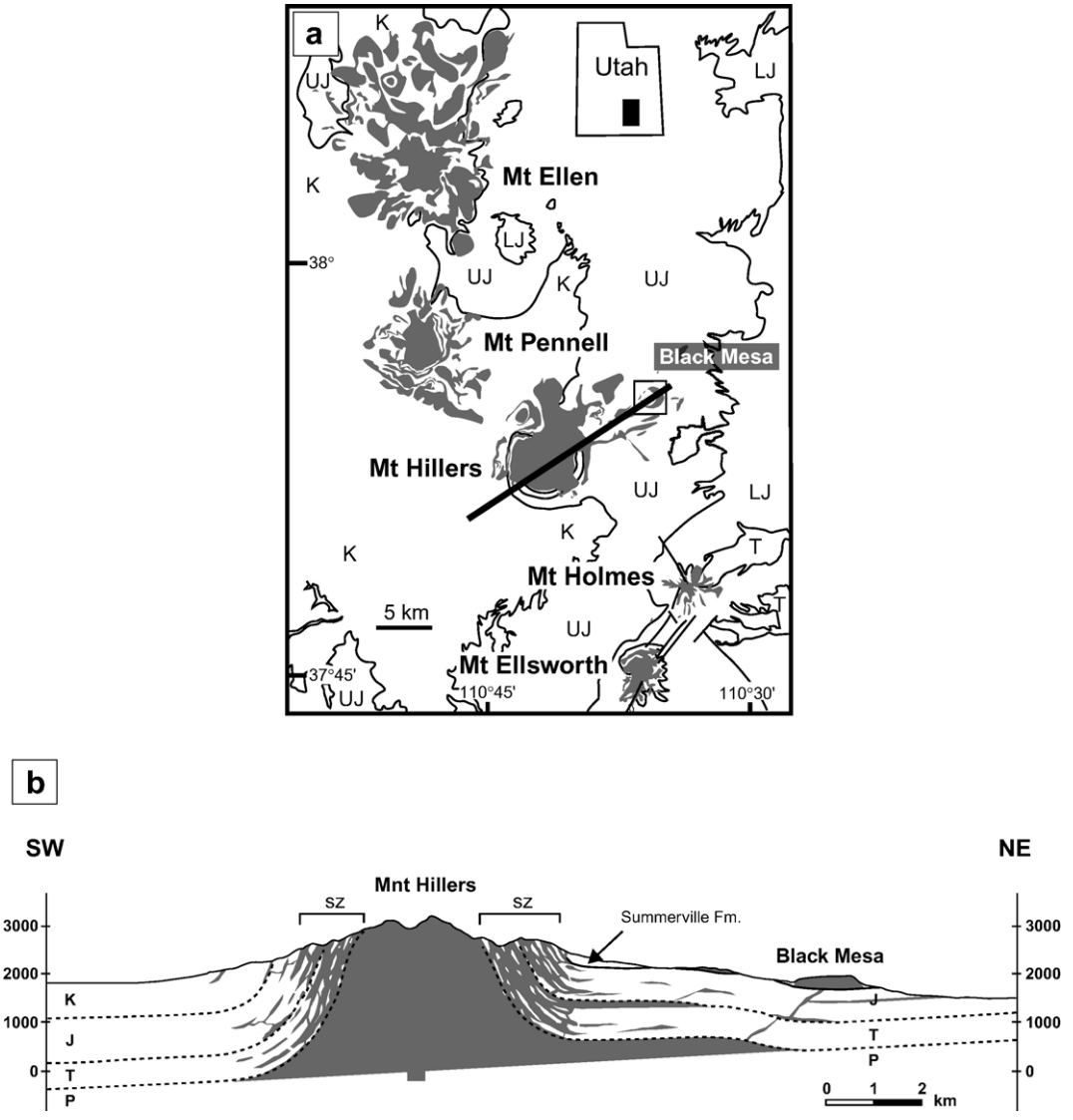

Fig. 1. Geological context of the Henry Mountains and the Black Mesa pluton: a) geological map and b) interpretative geological cross section from Mt Hillers to Black Mesa, based on the geological maps of Hunt (1953) and Larson et al. (1985), and our observations. The location of the cross section is represented by a bold line on the geological map. No vertical exaggeration. SZ shattered zone, P Permian, T Triassic, J Jurassic (L lower and U upper), and K Cretaceous formations.

they were far removed from the location of the Tertiary subduction zone (~1000 km), the Henry Mountains appear to be related to a large-scale igneous system with arc-like affinities (Nelson and Davidson, 1993, 1997). The relatively minor volume of igneous rocks on the Colorado Plateau compared to the contemporaneous regional magmatism of the same age may be due to the fact that the Colorado Plateau is underlain by a thick cratonic crust (Thompson and Zoback, 1979) which could have acted as a structural barrier and hampered the ascent of magma to higher crustal levels (Nelson and Davidson, 1993, 1997).

There are conflicting hypotheses for the geometry and emplacement mechanism(s) of the intrusive rocks of the Henry Mountains. It is clear that the radial disposition of satellite intrusions around the main domes show their mutual interrelation (Fig. 1). Hunt et al. (1953) interpreted the five major intrusions as stocks that fed the satellite intrusions laterally, while Jackson and Pollard (1988) proposed that the main intrusions are 'floored' large laccoliths that were emplaced after the smallest satellite intrusions. The latter hypothesis is in good agreement with rotated paleomagnetic vectors from the sills and the small laccoliths around Mt Hillers, which indicate that these intrusions cooled while still horizontal and were then tilted by the growth of the central main body, and is also in agreement with the regional aeromagnetic data (Jackson and Pollard, 1988).

3. The Black Mesa pluton

The Black Mesa pluton (BMp) is located on the eastern flank of Mt Hillers and intrudes within the upper part of the Summerville formation, just below the Morrison formation (Figs. 1 and 2). It is surrounded by the Sawtooth Ridge laccolith, which intrudes the Morrison Fm., and by the Maiden Creek sill (Horsman et al., 2005) and Trachyte Mesa laccolith (Morgan et al., 2005), which both intrude the Entrada formation. Based on an estimation of thicknesses of sedimentary rocks through regional stratigraphic correlation, the depth of emplacement of the BMp is estimated at 2.5 (from the section of Jackson and Pollard, 1988) to 2.7 km (Pollard and Johnson, 1973), based on the thickness of the overlaying series above the Summerville Fm. at the time of emplacement.

The BMp is a cylindrical pluton 1.7 km in diameter and between 150 and 250 m thick (Figs. 2 and 3). The intrusion is surrounded by sub-horizontal strata, which abruptly change orientation and become steeply dipping to sub-vertical at the contact. West of the intrusion, this folding is marked by a syncline (Fig. 3b); on the eastern half of the intrusion, the contact is characterized by vertical faults and is marked morphologically by a cliff (Fig. 3c). The roof of the BMp is flat, slightly north dipping, and generally covered by concordant sedimentary strata of the Morrison formation. The presence of this formation at the base and the top of the exposed diorite in a flat lying geometry led Hunt et al. (1953) to conclude that the floor of the intrusion must be close to the current bottom exposure. The volume of intrusive rock is then approximately between 0.3 and 0.5 km^3 if a cylinder shape is assumed.

Differential erosion between the sedimentary and magmatic rocks has produced a morphologically distinct intrusion (Fig. 3). The presence of valleys all around the BMp, except on the south-west where diorite rocks outcrop, lead Hunt et al. (1953) to envision lateral feeding of the BMp from the south-west, i.e. from the direction of the central Mt Hillers intrusion. The asymmetric form of the pluton, with its gently north-dipping roof and associated thickness increase from NW to SE (Figs. 2 and 3), can be attributed to the combination of: (1) a primary asymmetry developed during pluton growth; and (2) a tilt toward the NE due to the growth of Mt Hillers during and/or after BMp emplacement.

BMp is much studied (Hunt et al., 1953; Johnson and Pollard, 1973; Pollard and Johnson, 1973; Zenzri and Keer, 2001; Habert and Saint-Blanquat, 2004), because it seems to approximate the ideal laccolithic form conceived and defined by Gilbert (1877) in the Henry Mountains. Pollard and Johnson (1973) used the BMp to validate a general three-stage emplacement model for laccoliths: (1) the sill phase, controlled by lateral propagation of a thin igneous sheet, followed by (2) the laccolith phase, characterized by lateral propagation plus bending of the overlying sedimentary rocks, and finally (3) the bysmalith stage, during which lateral propagation decreases and further injection of magma is mainly accommodated by vertical lifting of the roof along a peripheral fault.

4. Wallrock structure

Wallrocks are mainly constituted by the reddish-brown mudstone and siltstone of the Summerville Fm, and the light-grey to light-brown sandstones of the base of the Morrison Fm. Only scarce evidence of recrystallization or growth of new metamorphic minerals was observed in the host rock, with some fracture planes filled mainly with albite atop the pluton and both albite and epidote above the margins and at the base of the pluton, indicating a temperature of roughly 400 °C. The sedimentary texture of the wallrocks is intact, even at the contact (Fig. 4a). This apparent absence of significant contact metamorphism may

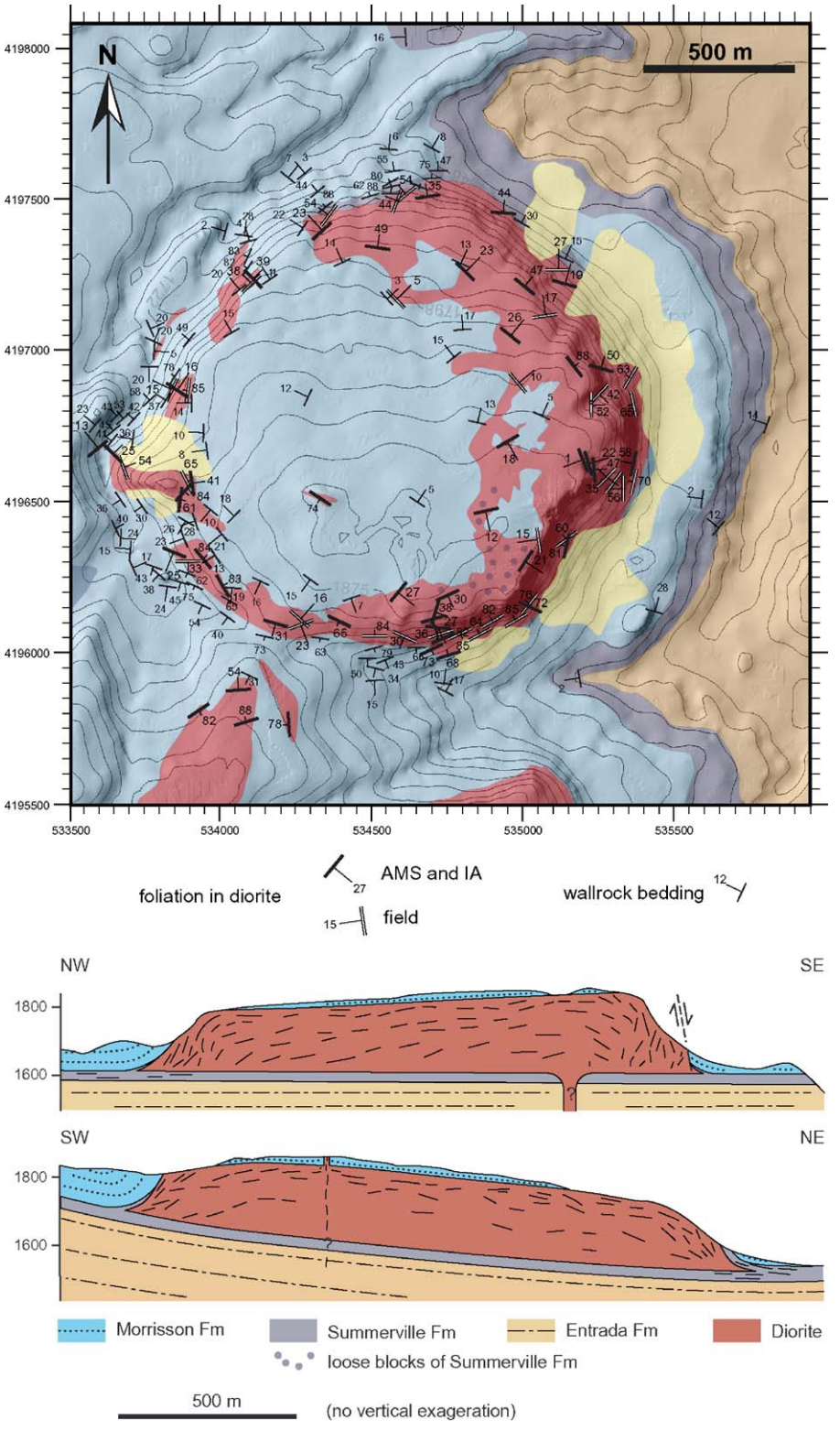

Fig. 2. Geological map (this work; topography from USGS; UTM coordinates; the grid is 500 × 500 m) and two perpendicular cross sections of the Black Mesa pluton; note the W–E asymmetry, the trace of foliations in the diorite, and the probable role of the mechanical anisotropy constituted by the interface between the Summerville (shales) and Morrison (sandstones) Fms. The position of the feeder dike is conjectural (see discussion).

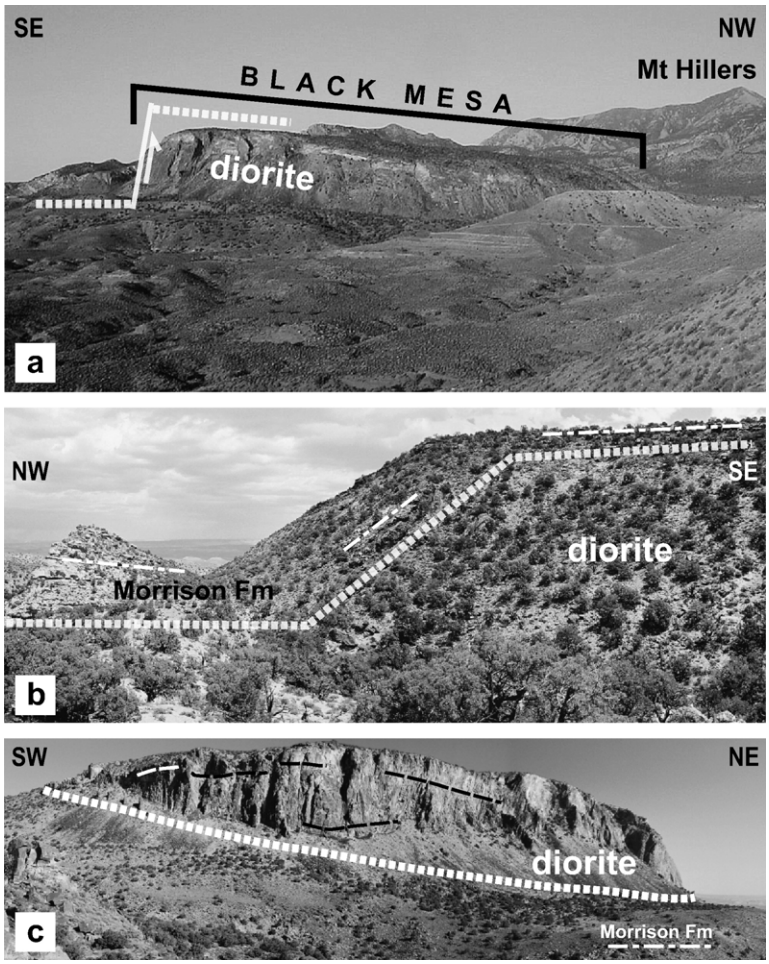

Fig. 3. Geometry of the Black mesa pluton; a) general view toward the SW; note the flat top, the NW–SE asymmetry, and the cliff which mark the contact along the eastern margin; b) view across the contact at the western margin; note the continuity of wallrocks and the monoclinal bending geometry. The white thick dashed line marks the geometry of the contact with the Morrison formation, and the dashed line mark the wallrock bedding; c) view of the eastern faulted contact; note the horizontal layering.

be due to a combination of a short thermal event, a low temperature increase during the emplacement, a refractory lithology (mainly sandstones with a low feldspar content) and the low H_2O content of the magma. Below, we examine the geometry and structure of wallrocks according to their position compared to the pluton.

4.1. Far from the pluton

Sedimentary rocks far from the intrusion are horizontal and undeformed. The only observable structural features are deformation bands and joints. Their regional orientation in the Morrison and Entrada Fms. is N60–80 and N120–140, both vertical (Larson et al., 1985; Bourroz et al., 1989; Jackson and Noller, 1991; Bergerat et al., 1992; this work).

4.2. Around pluton margins

The pluton margins can be divided in two distinct structural types, one along the eastern half and the other one along the western half of the pluton. The transition between them is gradational.

The east margin (Figs. 3c and 5b) is topographically distinct and is characterized by vertical cliffs of diorite, which mark the geometrical discontinuity of the wallrocks: they are horizontal up to approximately 100 m from the contact, then they are progressively rotated, until being vertical to slightly overturned at the diorite contact. Toward the base of the pluton, the contact is marked by steeply dipping normal and reverse faults with pluton-up movement, which separate moderately outward-dipping wallrocks from massive diorite deformed by horizontal

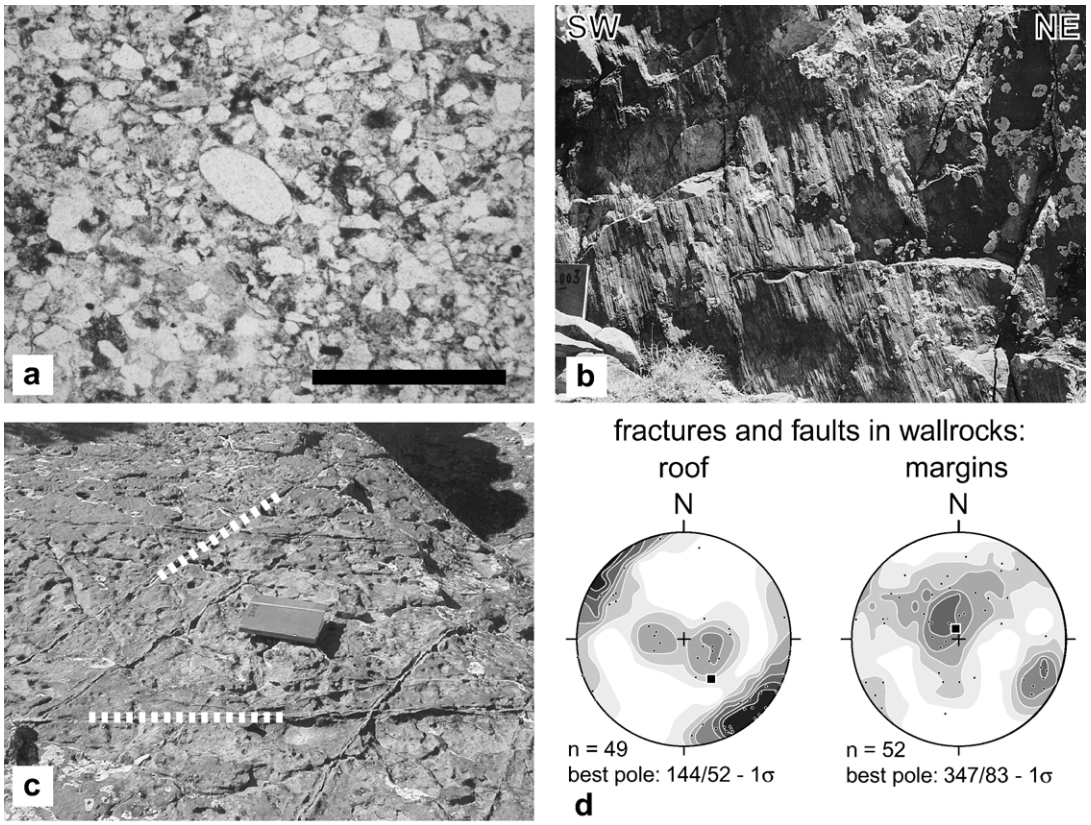

Fig. 4. Field observations of the wallrocks; a) texture of a sample of sandstone located 10 cm above the pluton's upper contact, note the absence of recrystallization, scale bar is 0.5 mm; b) faulted sandstone above the western pluton margin, note the sub-vertical striation; c) upper surface of a layer of sandstone from the Morrison Fm. above the top of the pluton, note the conjugate network of joints; d) stereograms of poles of fractures and faults above the pluton's roof, and above pluton's margins; see text for discussion.

and vertical cataclastic shear bands. Above, the wallrocks are more vertical, and the contact appears to be geometrically concordant (vertical wallrock bedding, i.e. parallel to the contact), but is marked by a network of anastomosing sub-vertical faults, both in wallrocks and in diorite (Fig. 8d). In general, the intensity of fracturing increases toward the more vertical part of the contact. The vertical wallrocks contain a network of shallowly dipping fractures and faults which could be interpreted as rotated remnants of the initial stages of faulting (Fig. 4d). Fault slip is generally down-dip.

Along the pluton's west margin (Figs. 3b and 5a), the sandstones of the Morrison Fm. are geometrically continuous from the top to the bottom of the pluton, despite detailed cross sections showing that the wallrocks are faulted (Fig. 4b and d). No cataclastic shears or faults were observed in the diorite. The contact has a staircase geometry which shows a monoclinal bending (e.g. Koch et al., 1981): two narrow hinges, one concave at the base, and one convex at the top of the pluton, separated by planar and outward-dipping beds of sandstone. The intensity of faulting is highest at the lower concave and upper convex hinges, and minimum or absent in the outward-dipping wallrocks between the base and the top of the pluton, which appear to be rigidly rotated.

4.3. Above the pluton

The wallrocks above the pluton are essentially undeformed aside from a network of joints, the main set of which is NE–SW and vertical, (Fig. 4c and d), i.e. perpendicular to the diorite cataclastic lineation at the upper contact. This family of joints sometimes contains albite mineralization. We note the presence of a set of conjugate shallowly dipping NNE–SSW joints, which always contains albite mineralization, which could be interpreted as the expression of a vertical flattening. No faults, and in particular no remnant of faulted hinge zones were observed. The only structures clearly associated with pluton construction are rare centimetre to decametre "horst and graben" structures. When observed, they are perpendicular to the diorite cataclastic lineation at the

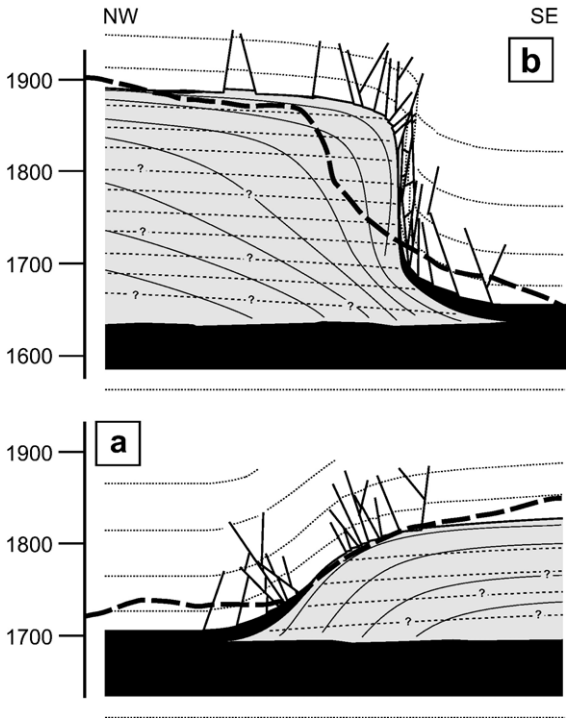

Fig. 5. Detailed synthetic cross sections of a) the north-west and b) the south-east contacts of the Black Mesa pluton. Black: Summerville Fm., grey: diorite, white: Morisson Fm. Dashed lines in the diorite: magmatic layering; thin line in the diorite: magmatic foliation. See text for description.

upper contact, and could be interpreted as the result of minor WNW–ESE extension. All the above structures were observed with a homogeneous spatial distribution over the pluton roof.

It is difficult to determine exactly how the wallrocks at the top of the pluton were affected by its growth. The orientation of the vertical family of joints is compatible with the regional joint orientation far from the pluton, but is also perpendicular to the cataclastic stretching lineation in the diorite at the contact, so could be also interpreted as the expression of an emplacement strain feature; the conjugate shallowly dipping joints and horst and graben structures can be similarly interpreted. We propose that the effect of magma emplacement on the wallrocks atop the growing pluton was only in the form of a fracturing without relative displacement and rotation of strata, and was homogeneously distributed over the roof surface, i.e., with no migration of deformation.

The structural study of wallrocks shows that, at first order, they have suffered no internal strain but only displacement by faults. The vertical upward displacement of wallrocks account for 100% of the space creation for magma. The deformation of wallrocks above and far from the pluton is similar, except for minor WNW–ESE extension recorded by low-dipping NNE–SSW joints and horst and graben structures.

5. Diorite

Hunt's (1953) geological map and cross sections show a BMp which intrudes between the "weak" middle Jurassic Summerville formation, and the base of the "strong" overlying upper Jurassic Morrison formations (Figs. 1 and 2). The presence of rotated red beds of the Summerville Fm. only around the northern part of the pluton lead Hunt to draw a cross section where the pluton intruded stratigraphically deeper toward the north. Our new detailed mapping shows that the initial level of intrusion is not exactly at the contact between the Summerville and the Morrison formations, but is rather located within the upper part of the Summerville Fm. We observed loose blocks of the Summerville Fm. at the top of the SE part of the pluton, and rotated beds of the same formation around the entire northern half of the pluton. The apparent absence of the Summerville Fm. around the southern half of the pluton could be a combined effect of both the talus cover and an extreme flattening of this soft layer due to the pluton construction. This new pattern clearly shows a lithological control on the level of intrusion.

5.1. Mineralogy, petrography, textures

A typical specimen of the BMp diorite porphyry has a microgranular porphyritic texture and consists of 50% of the following phenocrysts: 30% plagioclase ($An_{45–55}$, andesine–labradorite), 10% hornblende (edenite–pargasite), 5% clinopyroxene (augite),<5% magnetite, titanite and apatite. The groundmass, which is roughly 50% of the rock volume, is composed essentially of plagioclase, hornblende, and minor quartz (Fig. 6a). Fractures and some small miarolitic cavities are filled with calcite, quartz and epidote (Fig. 6b). The maximum phenocryst size is around 1 cm. Crystals in the matrix are generally smaller than 50 μm, and their size increases with decreasing elevation. Plagioclase phenocrysts show well-marked growth inclusions, synheusis, oscillatory zoning, and frequently have a sericitized zone between a fresh core and an outer fresh rim. Resorbed rims and overgrowths are uncommon. Hornblende phenocrysts are relatively homogeneous. The frequent observation of pyroxene, iron oxides, and plagioclase in aureoles around hornblende (oxyhornblende) (Fig. 6c) may be the product of a reaction between hornblende and melt, which produces a water loss. This reaction is generally interpreted as a consequence of a rapid adiabatic ascent

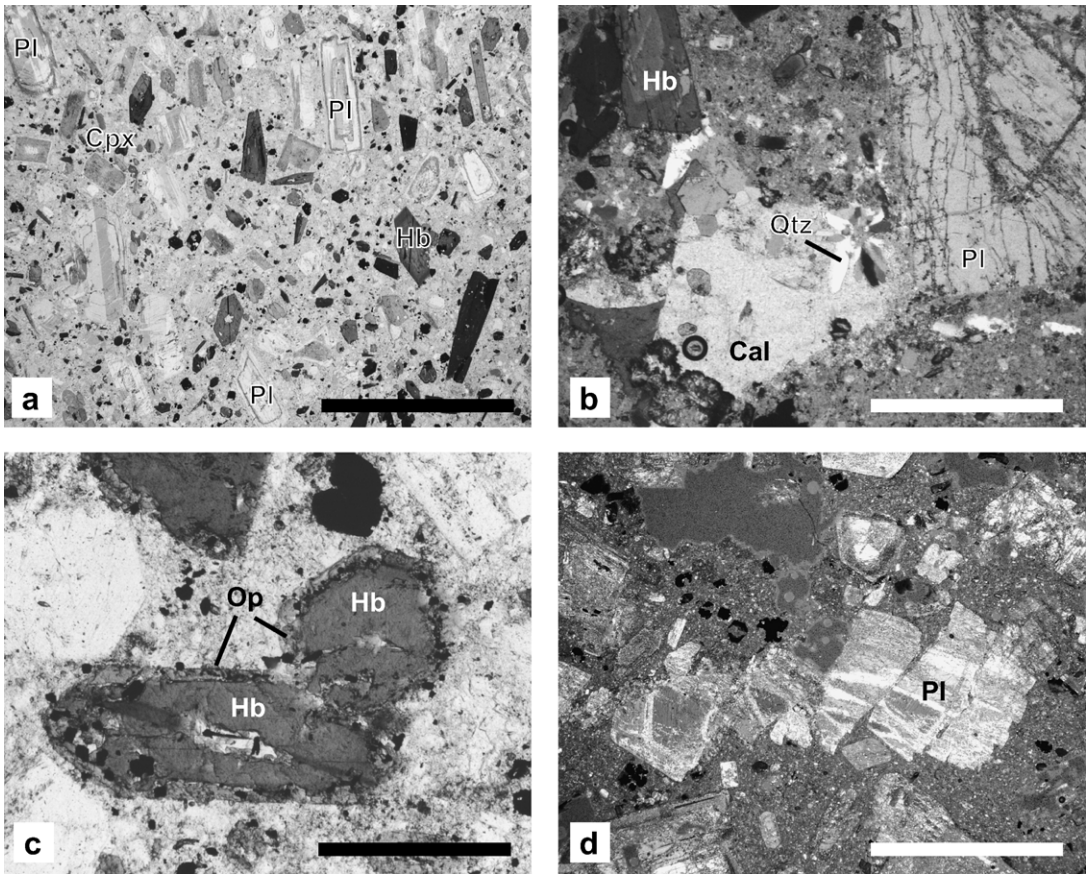

Fig. 6. Texture of the Black Mesa porphyritic microdiorite; a) general view of the magmatic texture; note the shape preferred orientation of the phenocrysts; scale bar is 5 mm; b) miarolitic cavities filled with calcite (Cal) and quartz (Qtz); scale bar is 0.5 mm; c) destabilization of hornblende into iron oxide (op), essentially composed of haematite; scale bar is 1 mm; d) cataclastically deformed plagioclase at the top of the pluton; scale bar is 2 mm. Pl plagioclase, Hb hornblende, Cpx augite, Qtz quartz, Cal calcite, Op iron oxyde.

from a deep reservoir (Rutherford and Hill, 1993; Nakada and Motomura, 1999). Augite is rarely stable and is often replaced by calcite. Qualitative studies of the spatial distribution of oxy-hornblendes and altered pyroxenes indicate that these textures are more abundant at the base of the magmatic body. Magnetite occurs as equant phenocrysts (Fig. 10a), as small grains in the groundmass, and as inclusions in hornblende (Fig. 6c).

Whole-rock analysis shows a bulk medium- to high-K calc-alkaline composition, with high alkali and CaO content ($Na_2O+K_2O=6.6–7.3$ wt.%; $CaO=5.3–6.5$ wt.%) (Appendix Table 1). The analyzed samples fall in the quartz–monzodiorite field in the QAP ternary diagram. REE shows a fractionated pattern ($(La/Yb)_N=9.3–9.8$), the absence of any wallrock contamination, and a clear arc signature. The BMp is petrographically homogeneous at the scale of the whole pluton: chemical analyses of six samples from a vertical section through the pluton show no significant petrographic zonation and a remarkable regularity from the base to the top, both for major and trace elements (Fig. 7). Chondrite-normalized REE patterns also show the remarkable homogeneity between samples. The only observed trends along the vertical profile are for Ca, Rb, and Sr, and could be related to very small modal variations in Ca-bearing phenocryst content. All these data argue for a short duration between intrusion of the earliest and latest magma batches, a short duration between the initial intrusion and the full crystallization of the pluton, and preclude the presence of any magma chamber process such as crystal settling at the level of emplacement.

5.2. Field observations of internal structure

The petrographic homogeneity of the BMp is associated with structural homogeneity at the scale of the whole pluton. Magmatic fabric in the intrusion is ubiquitous and is defined by the preferred orientation of

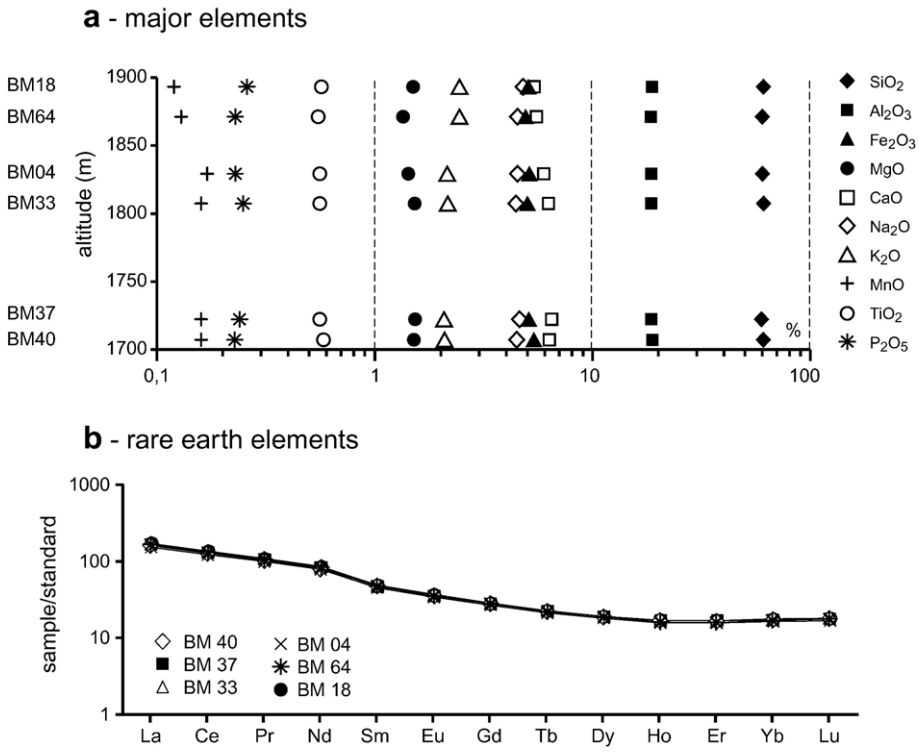

Fig. 7. Whole rocks petrographic data; a) major elements (weight %) versus sample elevation; note the log scale; b) trace elements normalized to chondrite; see text for discussion.

plagioclase and hornblende phenocrysts (Figs. 6a and 8a). Due to the needle shape of hornblende crystals and to the tabular shape of the plagioclase phenocrysts, the foliation is rarely well defined. The few locations where it was possible to get an accurate field measurement indicate different fabric orientations based on vertical position in the body. Sub-horizontal foliations occur at the top and the bottom of the intrusion, and steeper, inward-dipping foliations occur along the margins of the intrusion (Fig. 2). The preferred orientation of hornblende is the most obvious field structure and defines an easily measurable magmatic lineation (Figs. 6a and 8a). Both in the field and in thin section, magmatic textures were observed everywhere in the BMp, except in the outermost few centimetres of the diorite at the pluton–host rock contact, where cataclastic deformation was observed (Figs. 6d and 8b). At the vertical contacts along the SE margin, undeformed magmatic hornblende phenocrysts are aligned parallel to the vertical fault striations (Fig. 8d), showing the magmatic and cataclastic deformation had the same kinematics and consequently suggesting that the fault movement was syn-magmatic. Shear sense indicators show that magma moved upward relative to wallrocks during the emplacement, which is in agreement with the tilting of the surrounding wallrocks. The orientation of these faults is sub-vertical (Fig. 8d). From our dataset, it is not clear whether these faults are dominantly NE–SW-striking (stereogram of Fig. 8d), or if this pattern is due to an under-representation of NW–SE-striking faults, because of the absence of diorite outcrop on the SW margin of the BMp where only wallrocks are outcropping, and on the NE margin, where they are covered by talus.

Internal structures such as magmatic layering and internal contacts, defined by sharp variations in the relative proportions or by variations in the size of phenocrysts (Fig. 8c), were occasionally observed, particularly in the upper part of the pluton. These structures are typically sub-parallel to the magmatic foliation and/or pluton roof (stereogram Fig. 8c). They are not local small-scale features, but can be traced across large outcrops or in the landscape. In contrast to the adjacent intrusions of Trachyte Mesa and Maiden Creek, where cataclastically deformed plagioclase can be observed between successive injections (Horsman et al., 2005; Morgan et al., 2005), no solid-state deformation nor chilled margins associated with these features were observed in the BMp. However, on the east side of the pluton, close to the lateral margin and to the pluton roof, 1–2 metre thick horizontal layers of anastomosing cataclastic bands separated by 10–20 metre thick layers of undeformed and texturally homogeneous

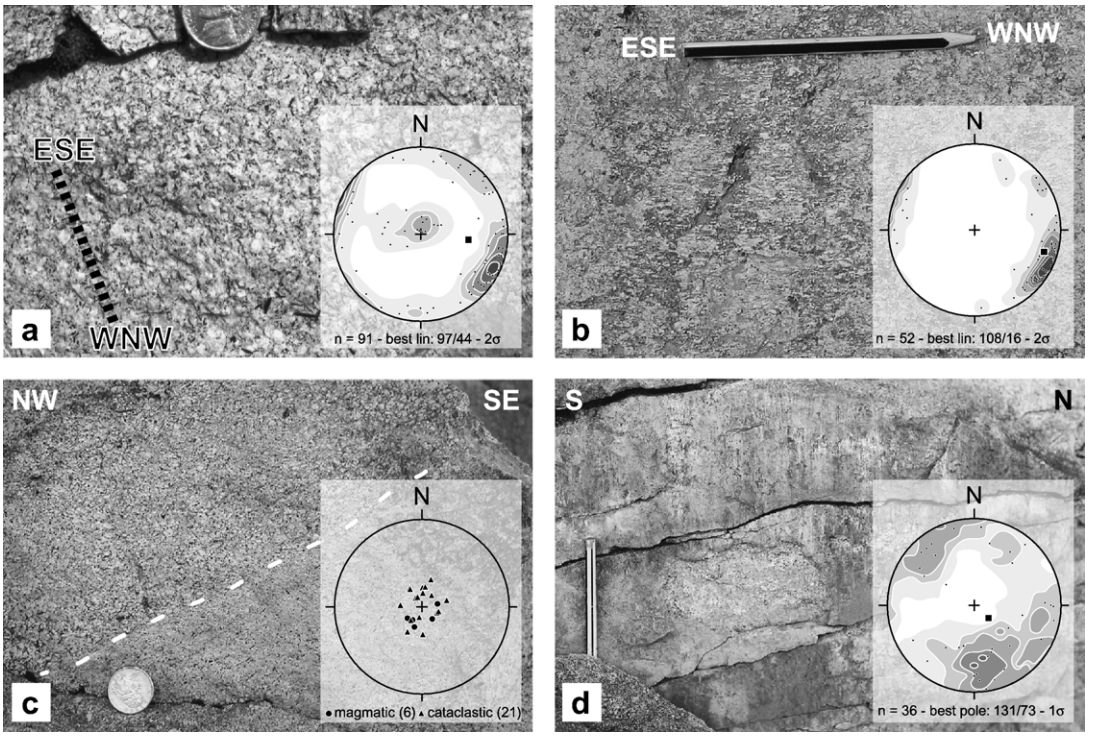

Fig. 8. Field observations of the diorite; a) field view of the diorite with a WNW–ESE magmatic lineation marked by the shape preferred orientation of hornblende phenocrysts (black dashed line); stereogram of the field-measured magmatic lineations; b) view of the upper contact of the BMp, marked by a WNW–ESE cataclastic lineation; stereogram of the field-measured cataclastic lineations; c) internal contact defined by an abrupt change in texture (white dashed line); stereogram of the poles of the syn-magmatic internal contacts and layering, and post-magmatic cataclastic bands; d) faulted diorite at the eastern margin; note the sub-vertical syn-magmatic striation; stereogram of the poles of all the fault planes measured in the pluton. All the stereograms in this figure and the following are equal area, lower hemisphere.

magmatic diorite are observed (see Fig. 3e in Habert and Saint-Blanquat, 2004). It is not clear if these structures are associated or not with magmatic layering as defined above. The absence of textural contrast on both sides, and their preferential location at the top of the eastern part of the BMp suggests that they represent mechanical boundaries that were cataclastically reactivated during injection of younger pulses toward the base of the pluton (bysmalith stage, see below). Rare vertical dikes of microdiorite were observed at the top of the intrusion. These observations and the small size of the observed miarolitic cavities in the BMp are in agreement with the emplacement of a fluid-poor magma at a shallow crustal level of approximately 2.5 km depth, as defined by the thickness of the overlying stratigraphic section (Hunt et al., 1953).

5.3. Magnetic fabric

The relationship between the mineral preferred orientation of a rock sample and its magnetic fabric depends on the nature of the magnetic (Fe-bearing) minerals, and on the textural relationships among the mineral grains (Stacey, 1960; Khan, 1962; Uyeda et al., 1963; Ellwood and Whitney, 1980; Rochette, 1987; Jover et al., 1989; Borradaile et al., 1991; Rochette et al., 1992; Grégoire et al., 1995, 1998). If a sample contains more than one magnetic mineral, the magnetic fabric becomes a composite of two or more subfabrics. Therefore interpreting anisotropy of magnetic susceptibility (AMS) data requires careful identification and characterization of all the magnetic minerals contributing to the AMS signal. In magnetite-type granitic rocks (Ishihara, 1977), like the BMp, the paramagnetic contribution of Fe- and Mg-bearing silicates is negligible with respect to the ferromagnetic contribution, because of the high intrinsic magnetic susceptibility of magnetite, so only the oxide minerals need to be carefully identified. However it is well known, that in plutonic rocks, oxide minerals can undergo sub-solidus re-equilibration (Frost et al., 1988; Frost and Lindsley, 1991). Thus the primary versus secondary nature of these minerals must be determined before any structural interpretation of the AMS signal of a rock sample is done. For our AMS analysis, accurately oriented hand specimens

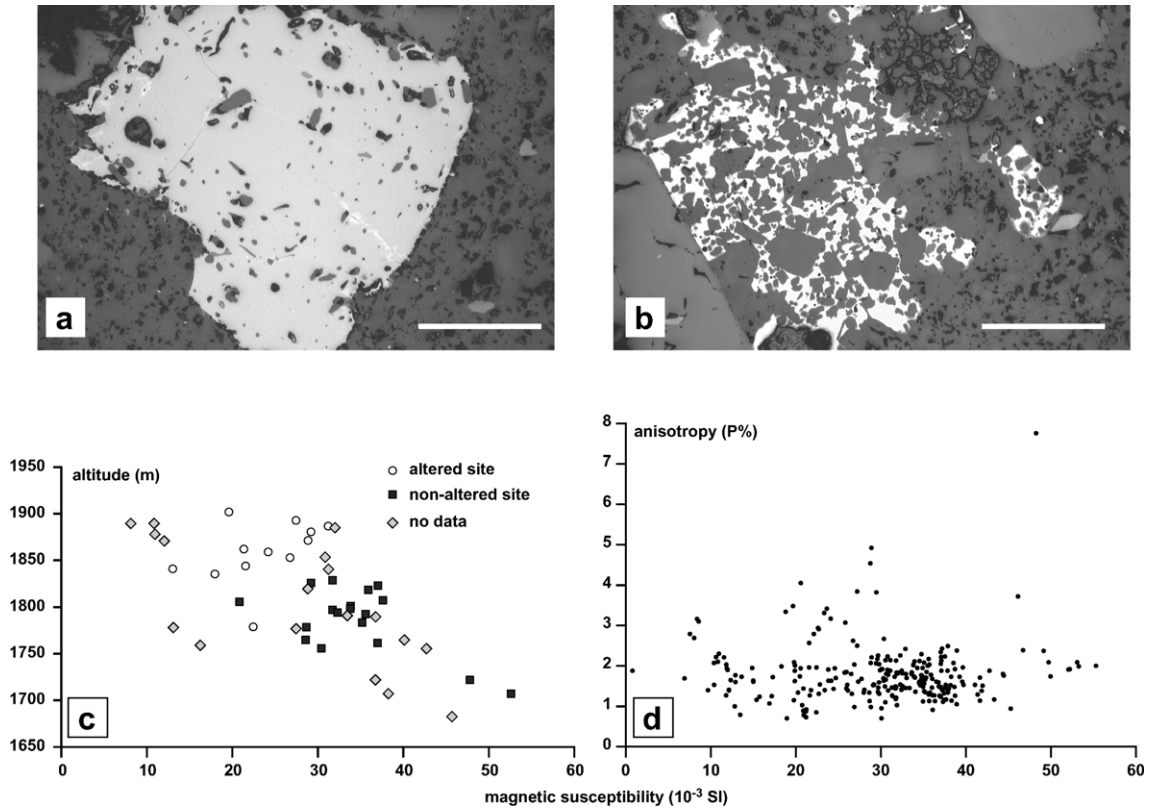

Fig. 9. Magnetic mineralogy; a) primary magnetite grain with growth inclusions (reflected light), scale bar is 0.1 mm; b) secondary goethite, scale bar is 0.1 mm; c) mean magnetic susceptibility plotted against the elevation for each sampling site; open circles represent samples on which partial Anhysteretic Remanence (pAR) revealed the presence of secondary magnetite grains; plain squares represent samples with a magnetic signal controlled by primary magnetite grains; grey lozenges represent samples on which no pAR has been done; d) plot of the magnetic susceptibility versus total anisotropy for all the samples, see text for discussion.

were collected from 50 stations covering the whole pluton. In the laboratory, 265 standard-sized (22×25 mm) cores were drilled from all hand samples with an average of 5 cores for each site. AMS measurements were made with a Kappabridge KLY-2 susceptibility metre working at 4×10^{-4} T and 950 Hz.

5.3.1. Origin of the magnetic signal

Opaque minerals in the BMp are composed essentially of euhedral 100–200 μm magnetite grains containing thin exsolution lamellae of illmenite. The euhedral shape of and growth aureoles in some large magnetite grains (Fig. 9a) support their primary origin. However, in some sites, secondary oxides like goethite are observed (Fig. 9b), and primary magnetite is partially replaced by haematite. These secondary oxides may be associated with late fluid circulation. To distinguish, we have measured the partial anhysteretic remanence (pAR) in 30 of our 50 AMS sampling sites. This technique isolates the remanence intensity of the ferromagnetic minerals. The highest AC field used during anhysteretic remanence acquisition and AF demagnetization was 100 mT. Therefore the remanence intensity cannot be related to haematite and goethite because of their much higher coercivities. In addition, since remanent coercivity in magnetite is grain-size dependent, primary coarse-grained magnetite and secondary fine-grained magnetite can be analyzed independently by using different intervals of magnetization. The lowest and medium coercivity fractions are ascribed respectively to coarse and fine-grained magnetite. The contribution of these different populations can be estimated from the remanent coercivity spectra, which correspond to the intensities of pAR acquired at intervals of 10 mT from 0–10 mT to 80–90 mT (see Trindade et al., 2001 for reviews). Measurements of remanence vectors were made with a JR5A magnetometer. Anhysteretic remanence acquisition and AF demagnetization were conducted using the LDA3-AMU1 apparatus. Our analyses distinguish two different types of sites, based on distinct coercivity spectra. The first type, where the magnetic carrier is coarse-grained magnetite, differs from the second type,

in which both the same coarse-grained population and a second finer grained population occur. These latter sites correlate with the altered samples recognized with the optical microscope. Therefore, we interpret this second magnetite population as the result of a late fluid circulation.

The finer grain magnetite population could result from primary magnetite grains partially transformed into haematite, which divide these grains into smaller portions and enhance their coercivity (Clark, 1997) or could be due to formation of new, finer grained magnetite during late fluid circulation (Trindade et al., 1999). This population of fine-grained magnetite was not identifiable by optical methods. We did not try to further identify the precise origin of the "altered signal" because we removed the corresponding sites from our structural interpretation. The sites with a significant population of secondary fine-grained magnetite were located at the top of the intrusion. In contrast, the samples with essentially primary coarse-grained magnetite were located inward (Fig. 9c) and have higher susceptibility values. In the absence of other highly susceptible minerals (e.g. pyrrhotite and maghemite), the intensity and orientation of AMS is determined by the elongation and shape preferred orientation of magnetite grains and clusters of magnetite grains (Gaillot et al., 2006). The magnetic fabric within the BMp was interpreted after identification of the status of magnetite in each site.

5.3.2. Intensity parameters

The mean magnetic susceptibility magnitude Km varies from 8 to 53×10^{-3} SI, with a mean value of 29×10^{-3} SI (Appendix Table 2); Km is relatively homogeneous at a given station from one sample to another with an average within-site variation of 4×10^{-3} SI. Within the intrusion, we observe a spatial organization with superposed sub-horizontal layers of similar susceptibility, along with a general decrease in susceptibility with increasing elevation (Fig. 9c). This pattern may be a primary feature due to the initial magnetite content of the magma. Alternatively, the pattern may be associated with late alteration close to the roof of the intrusion (see above). The total magnetic anisotropy $P\%$ (defined as $\{(K1/K3)-1\}\cdot100$) is very low, between 0.6 and 9.4% (mean value 1.8%) (Appendix Table 2), which corroborates the absence of solid-state deformation in most of the sites (Saint-Blanquat and Tikoff, 1997). This is also exemplified by the absence of global coupled increase of Km and $P\%$ (Fig. 9d). We note however the presence of a few samples having a high anisotropy (>4%), in which the presence of magnetic interactions may be present. But as recent experimental and theoretical work has shown that this effect is not quantitatively significant in granitic rocks (Gregoire et al., 1998; Gaillot et al., 2006), we envision the presence of a different magnetic mineralogy in these samples. Globally, the magnetic anisotropy increases toward the contacts, which may be attributed to magmatic strain accumulation at the pluton–wallrock interface. Since there is no correlation between susceptibility and anisotropy, this increase of $P\%$ toward the contact is probably a true qualitative finite strain gauge. The shape parameter T (mean value 0.16) shows high variability within each site and at the pluton scale. No clear pattern at the map scale could be determined, a common result in ferromagnetic plutons.

5.3.3. Directional parameters

In altered samples, the AMS ellipsoid represents the shape-preferred orientation of the small secondary magnetite grains, which may not necessarily be related to the primary magmatic fabric (Trindade et al., 1999). As we are focusing on the magmatic history (emplacement mechanisms), we disregarded the 13 altered sites during the interpretation of the directional fabric pattern. When it was possible (7 sites), we replaced the magnetic data of these altered sites by the SPO of hornblende phenocrysts determined by image analysis. Comparison of magnetic fabric and SPO at non-altered sites (not shown) demonstrate a clear agreement between the techniques, with, for example, the K1 axis sub-parallel to the long axes of the hornblende grains. Additionally, magnetic fabric is in good agreement to the field-measured fabric, where measured. When a discrepancy is observed, it is often for sites located very close (<1 m) to the contacts, where a rapid spatial change of the fabric pattern was observed. In these locations, we interpret field and magnetic measurements to be made at different levels and conclude that both are good representations of the rock fabric. Within individual sites, the magnetic fabric orientation is remarkably stable from one sample to another: the average within-site angular variation of both K1 and K3 is only 18°.

5.4. Internal structure of the BMp

5.4.1. Magmatic layering

The internal structure of the BMp is characterized by a sub-horizontal magmatic layering, defined by (1) sharp variation in the diorite texture, i.e. internal contacts, with a sub-horizontal orientation (Fig. 8c), (2) horizontal compositional layering (Fig. 3c), mainly evidenced by the magnetic susceptibility vertical profile (Fig. 9c) and by a weak vertical petrographic zonation (Fig.7), and (3) sub-horizontal internal structures (Fig. 2). The combination of these features suggests that the observed internal contacts can be interpreted as primary, and due to

discontinuous construction of the pluton, and not to secondary in-situ processes. Consequently, we infer that the pluton was constructed by the amalgamation of sequentially injected magma pulses. The fact that we can observe sheeting only at the pluton margins and not within its interiors can be interpreted as a thermal effect due to slower cooling of the interior relative to the margins.

5.4.2. Foliation

At the pluton scale, all the measured foliations (field, AMS, image analysis) (Fig. 2) are mainly sub-horizontal and define a flat outward-dipping dome-shaped pattern that is concordant with the pluton margins. More precisely, these foliations can be divided into four families: (1) sub-horizontal foliations (dip < 30°) on the very top of the pluton, (2) outward and moderately dipping (between 30 and 60°) foliations, along the pluton margins, (3) steep (> 60°), sometimes inward-dipping foliations, along the south-east margin of the pluton, and (4) vertical foliations in late vertical dikes on top of the pluton. The foliation pattern thus shows that the pluton margin exerted a strong influence on flow and deformation of the magma within the interior of the growing pluton. The controlling factor for the foliation is then the 3D geometry of the pluton.

5.4.3. Lineation

Lineations within the pluton can also be divided into four families (Fig. 10): (1) lineations on the very top of the intrusion are sub-horizontal and have a general WNW–ESE trend, (2) lineations from sites below the roof of the BMp have a NNW–SSE to NNE–SSW trend and moderate plunge (< 40°), (3) sub-vertical (≥ 70°) lineations along the south-east margin, and (4) vertical lineations within late dikes. On many sites on the top of the pluton, we have observed a progressive rotation of the lineation orientation from WNW–ESE at the contact to NNW–SSE or NNE–SSW farther away from the sub-horizontal contact. The vertical distance over which this rotation occurs is variable, from a few metres to 1–2 cm. For example, a very clear cataclastic WNW–ESE lineation was measured in the field at site no. 27, at the NW margin of the pluton, immediately underneath the contact, which is different from the NNE–SSW measurement obtained by AMS on a core taken between 5 and 20 cm below this contact. This kind of pattern can be interpreted in terms of the kinematics of magma infilling (see discussion below). The lineation pattern at the pluton scale shows that the internal fabric has a plane of symmetry that is oriented NNE–SSW and vertical.

5.4.4. Interpretation of the fabric pattern

The study of the mechanisms of emplacement of the BMp, deduced from its internal texture and fabric, is hampered by the fact that we have no access to the real core of the pluton. However, given that (1) we observe rapid and localized change of fabric orientation (rotation of the finite strain principal axes) only at the pluton contact and a homogeneous fabric pattern everywhere else (see above), and (2) the relatively simple circular and tabular 3D shape of the intrusion, we can reasonably hypothesize that no major changes of fabric pattern occur toward the pluton's centre.

The comparison of the foliation and lineation patterns allows us to propose a spatial partitioning of the internal fabric of the BMp in four main zones. Domain 1 is located on the very top of the pluton, where we have observed WNW–ESE magmatic and cataclastic lineations, associated with sub-horizontal, contact-parallel foliations. Domain 2 constitutes the main body of the pluton, and is characterized by a magmatic fabric with sub-horizontal to outward-dipping foliations and sub-horizontal to moderately plunging NNE–SSW lineations. Domain 3 is located along the east and south-east margin of the pluton, and characterized by sub-vertical to inward-dipping foliation associated with sub-vertical lineations; there are also sub-vertical cataclastic faults that indicate a shear sense consistent with upward movement of the pluton relative to the wallrock. Domain 4 is constituted by rare late-stage WNW–ESE dikes of microdiorite, characterized by sub-vertical foliations and lineations, that cut all the previous types of fabric.

Several observations allow us to chronologically interpret this spatial variation of the internal fabric. These observations include (1) the geometry of the wallrocks, which show clearly their vertical displacement due to the growth of the pluton, and consequently imply under-accretion of magma pulses; (2) the mutual cross-cutting relationships and relative position of the four different fabric domains; and finally (3) our data from other adjacent sills and laccoliths (Horsman et al., 2005; Morgan et al., 2005). Considered together, these observations allow us to infer a relative chronology from domain 1 to the latest pulses in domain 4. At the top of the pluton, domain 1 contains the oldest fabrics that were formed during the intrusion of the very first magma pulse, and then show the strain record associated with the initial sill emplacement. Domains 2 and 3 cannot be separated temporally based solely on structural data; they are volumetrically the more important and contain an "inflation" fabric formed during pluton growth accommodated respectively by wallrocks' bending,

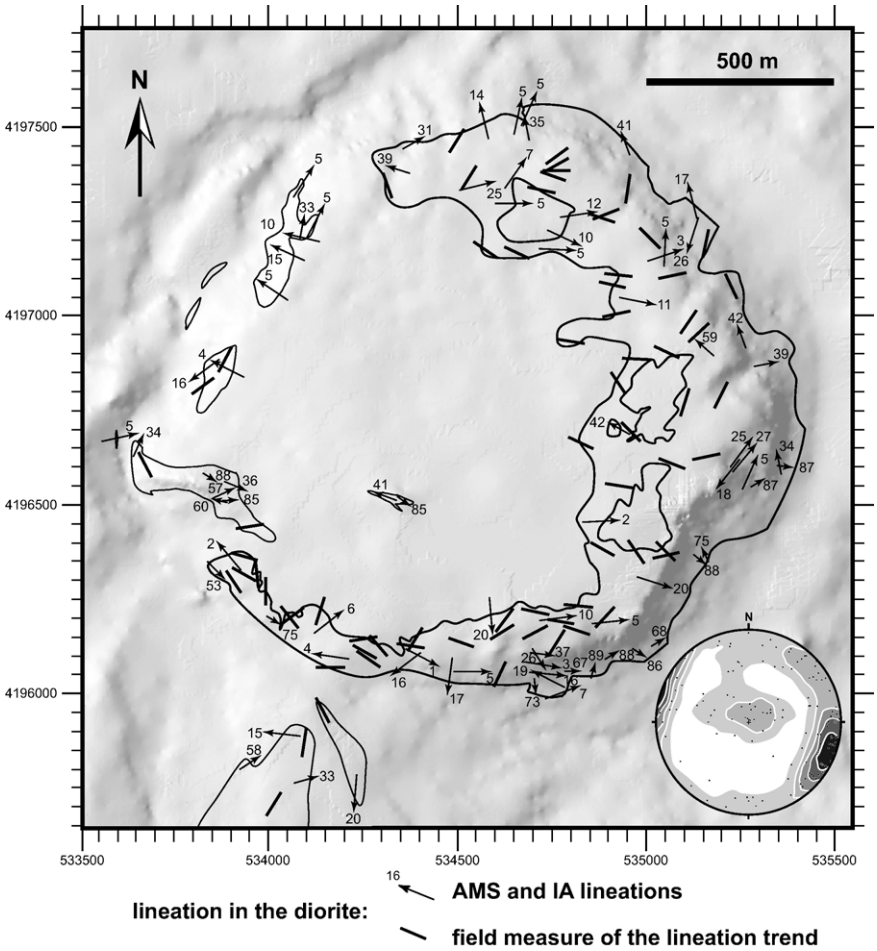

Fig. 10. Map of the lineation within the diorite, from the compilation of all types of data (field, AMS, Image Analysis, and corresponding stereograms (Schmidt, lower hemisphere); topography from USGS, geology, this work; same caption as Fig. 2. See text for discussion.

faulting and rotation in domain 2, as observed now in the west part of the BMp, and by roof lifting along peripheral faults in domain 3, as shown by the association of vertical magmatic lineation foliation and the vertical pluton-up faults along the south-east margin of the pluton. Finally, the dikes of domain 4 cross-cut all of the above fabrics, represent the latest intrusion within the pluton, and are thus the youngest features.

6. Discussion

6.1. Mechanism of Black Mesa pluton emplacement (Fig. 11)

6.1.1. Location and geometry of the feeder

The two previous hypotheses about the feeder of the pluton were from Hunt et al. (1953), who favoured a lateral injection from the SSW and from Pollard and Johnson (1973), who favour a vertical dike below the BMp. The main observation presented in support of a lateral feeder is the presence of a diorite ridge, mapped as sediments by Hunt et al. (1953), and located at the SSW end of the pluton and in apparent morphological continuity with it. Our detailed mapping has shown that these two bodies are in fact separated by steeply dipping beds of the Morrison Fm. (Fig. 2a). This result is corroborated by a SW–NE gravity profile we conducted across the BMp (not shown), which shows that this gap between the two intrusions is not only superficial, but continues at depth. Moreover, the two bodies have different phenocryst contents, and are of slightly different petrographic facies. Other main observations against a lateral feeder and in favour of a feeding from below are: (1) the symmetry of the internal fabric, as a lateral feeder should produced a lineation pattern pointing toward the feeder, presumably toward the W or the SSW, and an arcuate foliation pattern; neither of these features is

observed, and (2) the 3D cylindrical shape of the intrusion. The NNE–SSW plane of symmetry of the internal fabric pattern strongly suggests a planar feeder, i.e. a dike. We have no clear evidence regarding the orientation of this dike, which could be either NNE–SSW or WNW–ESE, but a NNE–SSW orientation is more compatible with the strain record at the top of the pluton. In either orientation, the feeder dike could be either vertical or inclined. The asymmetry of the 3D shape of the pluton, with its thickness increase from west to east, suggests a NNE–SSW planar feeder, not exactly in an axial position but in a slightly off-axis position toward the east (Fig. 11).

6.1.2. Sill stage

If our model of accretion of magma pulses from below (and not laterally) is correct, then the upper part of the pluton represents the oldest pulse. Consequently, the kinematics at the pluton–wallrock interface represents the kinematics of the initial magma intrusion. In this case, the WNW–ESE magmatic and cataclastic lineations at the top of the pluton are the record of the first relative movement between the magma and the wallrocks during the formation of the initial sill within the upper part of the Summerville formation. The parallel, non-radial pattern of cataclastic lineations shows that the sill was filled from a linear rather than a point source, i.e. a NNE–SSW oriented dike. Due to the strong temperature contrast between magma and host rocks at that time, the external part of the first pulse was chilled and cataclastically deformed during sill growth. The foliations within the evolving sill would have been oriented parallel to the sill plane, i.e. parallel to the sub-horizontal sediments. Close to the sill margin, and induced by the lateral propagation of the intrusion, the fabric could rotate to be more parallel to the contact. The thickness of this sill is unknown, but the observation of the neighbouring Trachyte Mesa and Maiden Creek sills suggest that the thickness of individual pulses is in the order of 10 to 30 m. It should be noted that the sill occupies a particular structural position, as it is located at a weak interface, the Summerville Fm., between two rigid layers of sandstones, the Entrada Fm. below and the Morrison Fm. above.

6.1.3. Sheeted growth stage

Except for the very first centimetres to metres, there are no major structural changes between the upper part of the pluton (the initial sill) and the layers situated below. This observation suggests that, after the initial sill intrusion, the mechanism of growth did not change radically during emplacement. Thus, either all the magma was injected after a single pulse or the body consists of a series of sheets that either coalesced or show similar fabrics. We support the latter model, primarily because of our field observation of distinct sheets in the pluton and in the nearby smaller igneous bodies (Maiden Creek, Trachyte Mesa). The absence of solid-state deformation around all the observed magmatic layering and internal contacts within the BMp indicates that the time gap between individual injections was insufficient to allow a complete solidification of the older pulse before the emplacement of the younger one.

We distinguish between a “sheeted” growth and “single pulse” growth, depending on whether magma intrusion contains multiple pulses or a single pulse to control pluton emplacement. In the sheeted growth model, the final horizontal size is mainly achieved at the end of the intrusion of the initial sill, and bending of wallrocks occurs only at the tip of the intruding pulse. The wallrocks suffer mainly vertical translation, and only minor thinning because of the small area increase. This forcible emplacement mechanism is mainly indicated for the BMp by (1) the foliation pattern and its concordance with the pluton–wallrock contact, (2) the deformation pattern within and around the pluton, and (3) the syn-magmatic nature of deformation at the pluton margin. Our proposed kinematic model is that each pulse of magma intruded horizontally below the previous one, nearly at the base of the growing pluton. The overlying, already-intruded sheets and wallrocks are mainly uplifted, and only slightly deformed by subsequent magma intrusions. Due to the strong margin control, the magmatic foliation dip increases toward the external contact. The magmatic lineation is parallel to the feeder long axis in the pluton centre and parallel to the contact at the pluton margins. We note that the control exerted by the contact was less marked in the north part of the pluton, where the lineation remain NNE–SSW, i.e. parallel to the feeder horizontal long axis. A slight bending and thinning is observable in this “cap” of pre-existing, overlying intrusion by (1) the curvature of the lineation pattern at the top of the pluton, (2) the elliptical shape of the foliation pattern, and (3) some shear criteria and small-scale horst and graben structures at the upper contact.

6.1.4. Faults-assisted growth stage

Margins of the BMp are not similar all along the pluton’s periphery. The margin along the eastern half of the intrusion is marked by peripheral faults, which have accommodated most of the roof lifting, whereas the margin along the western half is simply marked by a syncline and by an apparent continuity of wallrocks at the pluton scale. The “bysmalithic” faults assisted growth stage phase is therefore more complex than previously described by Hunt et al. (1953) and Pollard and Johnson (1973), and a simple piston model is not appropriate. The

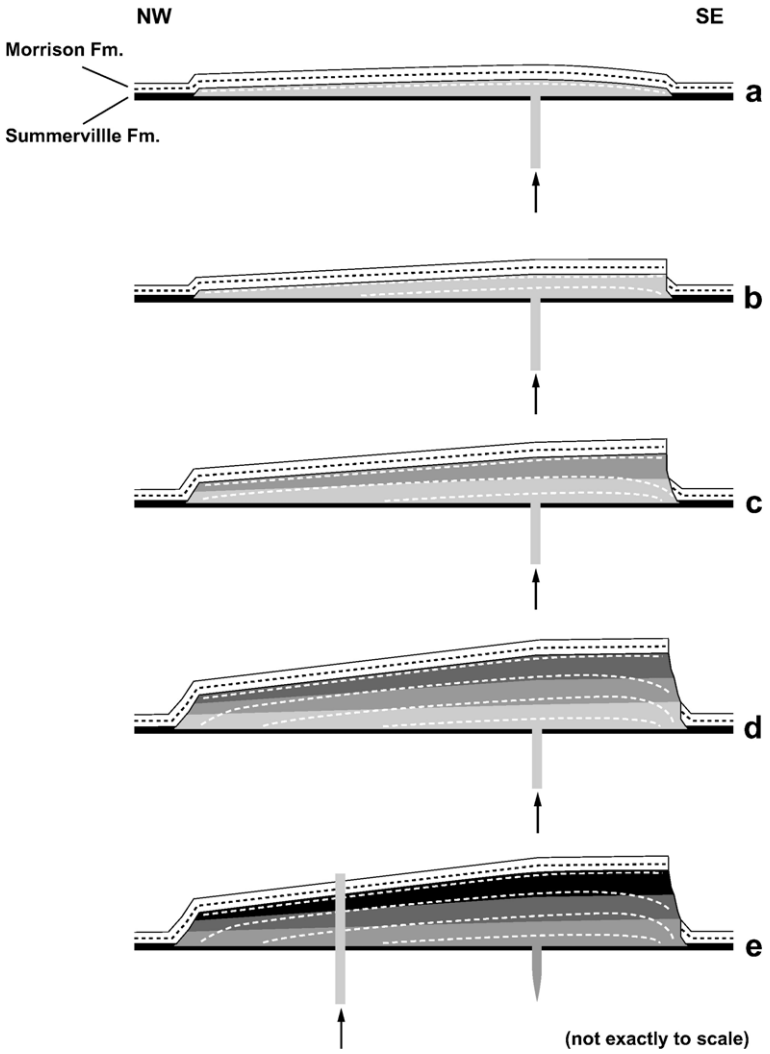

Fig. 11. Proposed model for the construction of the Black Mesa pluton; see text for discussion.

lineation along the eastern margin is sub-vertical, and the foliation is parallel to the contact and sub-vertical to steeply inward dipping. The very last pulses are in the form of E–W to WNW–ESE dikes visible on the top of the BMp, cross-cutting all the previous structures and containing fabrics that indicate vertical flow of magma. These structures are markedly different from those observed in the western part of the pluton and probably are the result of a different emplacement mechanism (e.g. "bysmalith" versus "sheeted laccolith"). This change in the mode of space accommodation between the sheeted growth and the fault-assisted growth stages may be the result of dissimilar magma supply rates in the different parts of the pluton. The input of more magma in the east may have induced a rupture in the continuity of wallrocks and the development of margin parallel faults, producing the asymmetric pluton geometry we observe. The origin of this asymmetry in magma input can be explained by an asymmetric position of the feeder (see above).

In summary, the study of the 3D geometry, composition, internal structure, and microstructures of the BMp allow us to propose an original emplacement model, which is characterized by (1) a multi-pulse construction by under-accretion, (2) an asymmetric sheeted growth mechanism, and (3) the maintenance of a molten zone at the base of the growing pluton. These results will be used to constrain the duration and rate of BMp emplacement with the help of a thermal numerical simulation.

6.1.5. Comparison with previous models

Our model is in general agreement with the emplacement model of Pollard and Johnson (1973),

which was mainly based on wallrock geometry. This model involves the following three stages: (1) sill intrusion and growth by lateral propagation, (2) when a critical length/thickness ratio is achieved, the sill begins to inflate vertically by overburden bending to produce a laccolith, which is also still growing laterally, and (3) fracturing of wallrocks over the periphery of the intrusion permits the uplift of both the sedimentary cover and older igneous sheets. This fault-controlled roof uplift results in vertical growth and transforms the laccolith into a bysmalith.

However, some differences between Pollard and Johnson's (1973) model and our observations remain. First, we find no clear evidence for a true laccolithic stage, for the three following reasons: (1) the simultaneous vertical and lateral propagation is not supported by our data, which show an initial sill that had a final size similar to the final horizontal size of the pluton; (2) the BMp displays a tabular, nearly flat roof, not a dome-like shape predicted by laccolithic growth; and (3) the profile of the contact on the west side of the BMp has a sharp staircase shape rather than a smooth progressive "laccolith-like" bending. These observations are compatible with a sheeted laccolith growth model, as defined by Morgan et al. (2005) for the neighbouring Trachyte Mesa laccolith. This model explains pluton growth through vertical stacking of sill-like magma sheets which cause the overlying wallrocks to bend upward and become slightly stretched and thinned. But as the final thickness of the Black Mesa pluton is ten times the thickness of the Trachyte Mesa laccolith, the bending, stretching and thinning of the wallrocks are minor in Black Mesa in regard of the space created by the faulting and rigid rotation of wallrocks.

The second difference is that our model explains the symmetry of the internal fabric within the pluton, with its implications for the spatial and temporal organization of the inflation stages. The east side of the pluton has the characteristics of a bysmalith, while the west side has the characteristics of a sheeted laccolith, but no true chronological order can be made between them from structural data. Thus, bending on the west and lifting on the east could in fact have occurred simultaneously, rather than successively. Consequently, the fault-assisted growth stage is not necessarily the record of an increase of the infilling rate, but may be simply the expression of a greater volume of magma intruded in the eastern part of the pluton, due to the asymmetric position of the feeder (see above).

The final difference is that the idea of the achievement of the maximum horizontal size before the beginning of vertical growth is also supported by the wallrocks structural data. First, the absence of faults (i.e. "remanent" hinges) in wallrocks above the pluton shows that the deformation remained localized more or less at the same place (along the margins) during pluton growth. In other words, the vertical growth began after the lateral growth, and then consequently the vertical growth was not accompanied by a significant lateral growth. Second, in the marginal wallrocks, we have measured not only sub-vertical, but also sub-horizontal and shallowly dipping fractures and faults, with normal and reverse slip sense. These can be interpreted as remnants of flexural hinges developed during the beginning of the vertical growth, before the loss of continuity of the bedding (see Fig. 16 of Corry, 1988).

6.1.6. Kinematic interpretation of the fabric pattern: magma infilling (Fig. 12)

We observe a very rapid change in the finite strain pattern within the first few centimetres or metres below the upper contact of the pluton. The relative displacement between host rocks and the first magma pulse is recorded by a WNW–ESE lineation that is cataclastic at the contact. A few centimetres below the contact, this lineation gradually changes character and becomes a magmatic fabric, rather than a solid-state fabric. We interpret this fabric to record the relative displacement between the first intrusive pulse of magma and the overlying wallrock. As we explain in more detail below, the gradual change from solid-state to magmatic fabric probably reflects the strong thermal contrast between the magma and the host rock immediately adjacent to the contact, along with the fast strain rates that develop at such contacts.

At greater distances below the upper contact, the magmatic lineation rotates progressively to a NNE–SSW orientation. We believe this lineation orientation records the stretching direction within the flowing magma, rather than the relative displacement between the flowing magma and the wallrock. This interpretation implies that within less than a metre the magmatic flow becomes essentially unaffected by the kinematics at the upper contact. The distinction between the different fabric development environments is explained in Fig. 12 based on distance from the upper contact. Within a few tens of centimetres of the contact, the fabric records the magmatic flow direction (particle paths on Fig. 12) away from the long axis of the suspected feeder dike. As the thermal gradient within the magma decreases, fabric orientation remains consistent but changes from solid-state to magmatic in character. At greater distances from the contact, fabric records the stretching direction within the magma itself (strain ellipses in Fig. 12a). Because the magma is diverging away from the feeder, the stretching direction is at a high angle to the flow direction of individual particles.

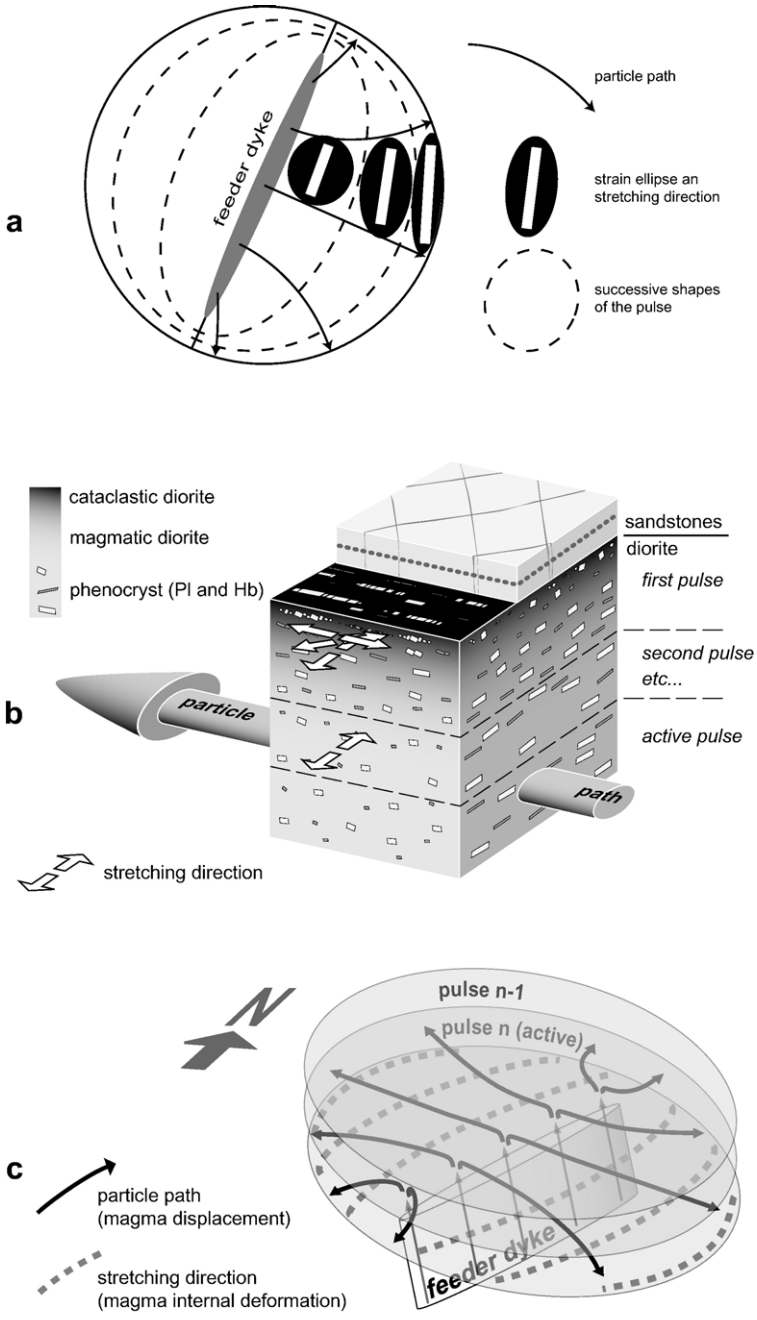

Fig. 12. a) Theoretical relation between strain and flow in a growing sill; b) kinematic interpretation of the internal structure (outcrop scale); c) kinematic interpretation of inflation of the pluton (pluton scale); not exactly to scale; see text for discussion.

We propose that the kinematic history of magma emplacement is constant throughout the history of the BMp — magma is always flowing out away from the feeder dike (Fig. 12c). However, the strain record of this single, simple kinematic framework changes depending on the proximity of the wallrocks. The temperature gradient is large between the top of the first intruded sheet and the relatively cold wallrock. Consequently, the viscosity of the magma is relatively large near the contact and fabric (both solid-state near the contact and magmatic farther away) develops sub-parallel to the WNW–ESE magma flow direction as the magma 'drags' viscously against the wallrock. Farther from the contact, the relatively high-temperature magma is much less viscous,

strain gradient is low, and individual crystals align with the stretching direction in the magma as it flows out and away from the dike. Subsequently intruded sheets flow adjacent to overlying recent sheets, temperature gradients are low and fabric again records stretching direction in the magma. Thus, the major external control on fabric development appears to be the temperature gradient within a given sheet. The fabric patterns we observe are likely the product of high frequency of intrusive pulses that serve to maintain a permanent magmatic zone at the base of the pluton. Similar observations of such rapid spatial changes of deformation control have been made on other intrusions (e.g. Liss et al., 2002). The presence of a permanent magmatic zone also provides an explanation for why we do not see the contacts between sheets in the pluton interior, a common observation in many plutons.

6.2. Duration of Black Mesa pluton emplacement: thermal numerical simulations

6.2.1. Principle

We have attempted to constrain the duration of BMp emplacement by modelling the thermal evolution of the growing pluton and its wallrocks for different emplacement scenarios. The two characteristic parameters we used to constrain the time and rate of emplacement are the time between each injection, t_i (or frequency of pulse intrusion), and the thickness of each injection, h (equivalent to the number of pulses). The geometry of the model is based on the results of our structural study (under-accretion, sheeted growth, etc., see above) (Fig. 13). The results were obtained by comparing the modelled temperature profiles with two petrostructural constraints: (1) the absence of solid-state textures around internal contacts, which implies that a melted zone was maintained in the intrusion during its emplacement, and (2) the absence of significant contact metamorphism or recrystallization, which means that the increase of temperature in the host rock was relatively small, or short-lived, or both.

6.2.2. Methodology

Given the relatively simple cylindrical geometry of the pluton, and the ratio of 1 / 8 between the thickness of the body and its lateral extension, we consider that the approximation of the infinite plane can be used to explore the evolution of the temperature of a vertical line in the middle of the pluton. Therefore, we used a one-dimensional model. The thermal history of the emplacement of the intrusion and its surroundings has been numerically simulated with the program DF1DEXPL.vba which is a visual basic code, based on an explicit finite difference algorithm to solve the one-dimensional conductive heat transfer equation (Peacock, 1990; Gvirtzman and Garfunkel, 1996):

$$\frac{\partial T}{\partial t} = \frac{k}{\rho C_\mathrm{p}} \frac{\partial^2 T}{\partial z^2} + \frac{A(z)}{\rho C_\mathrm{p}} \tag{1}$$

where T is temperature, k is thermal conductivity, t is time, $A(z)$ is internal heat production rate per unit volume, z is depth, C_p is the specific heat per unit mass and ρ is the density. The latent heat (ΔH) is computed using the formulation of Furlong et al. (1991). At each node, if the temperature belongs to the interval of crystallization ΔT ($T_\mathrm{liquidus} - T_\mathrm{solidus}$), the latent heat is included in the specific heat with the formula (Furlong et al., 1991):

$$C_\mathrm{p\_modified} = C_\mathrm{p} + \frac{\Delta H}{\Delta T} \tag{2}$$

Parameters for the magma and the host rocks are given in Fig. 13. The boundary conditions are the same for all simulations: (1) there is no heat flux at the boundaries, and (2) the boundaries of the model are far enough from the intrusion that they are not influenced by the heat release from the magma (i.e. the boundaries stay at the same temperature during the entire simulation as there is no internal heat production in the host rock). We note, however, that the temperatures we obtain are overestimated, due to the fact that heat transfer is only conductive and that there is no 3D dispersion of heat. One way to use this model is then to look at *relative* differences from one simulation to another. To be able to compare the different simulations, we let the model evolve until external contacts cooled to a temperature of less than 500 °C.

Previous work (Johnson and Pollard, 1973) assumes that emplacement of new injections occurs from below, at the base of the intrusion, with an upward vertical displacement of the pluton roof. This geometry is suggested by our data on the geometry of the wallrocks and by the internal fabric of the pluton. Therefore, we chose to emplace the incoming magmatic pulse below the earlier pulses (under-accretion), but, as there is necessarily a part of the first intrusive sheet that is frozen right at the contact, new injections are emplaced at a certain distance above the lower contact with the underlying wallrock. We fixed this distance by referring to the first stage of the emplacement where a sill propagates between the Morrison and Summerville formations. Injections are emplaced at the middle of the sill. As sills around the BMp, and in the Henry Mountains in general, have a mean thickness of 20 m (Johnson and Pollard, 1973), new

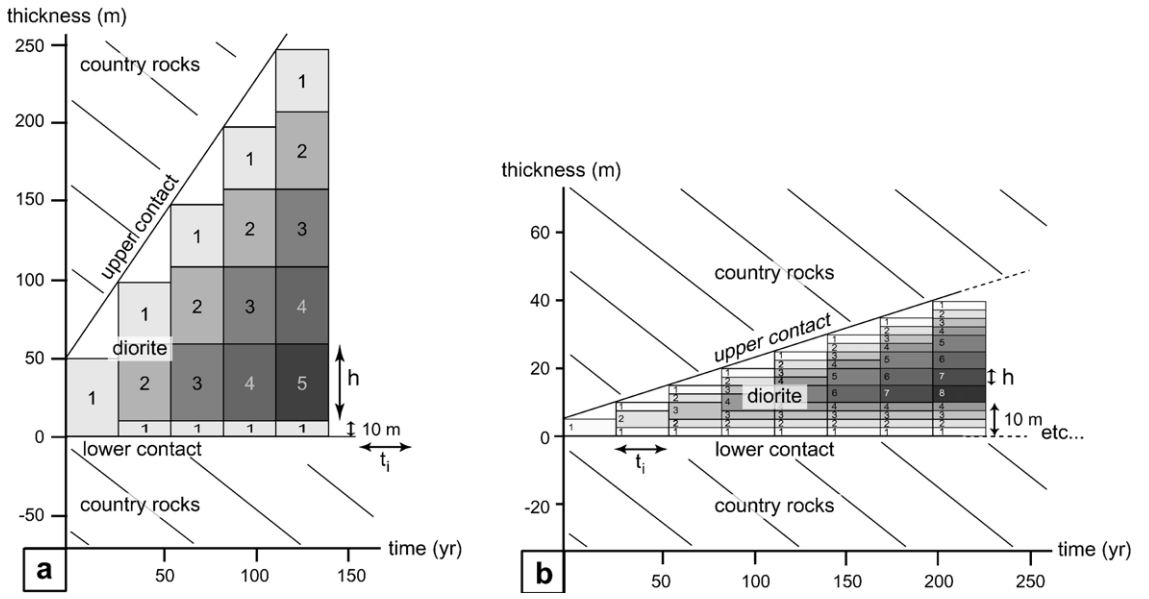

Fig. 13. Principles of the numerical models; a) for injections thicker than 20 m; b) for injections thinner than 20 m; h pulse thickness, t_i time between successive pulses. Thermal parameters for the wallrock and diorite respectively: specific heat 1000 and 1100 J kg^{-1} K^{-1}, thermal conductivity 2.65 and 3 W m^{-1} K^{-1}, density 2630 and 2730 kg m^{-3}, and for the diorite only, latent heat of crystallization 290000 J kg^{-1}, crystallization interval 200 °C, solidus temperature 700 °C.

injections are placed at 10 m from the lower contact (Fig. 13a). For models where the thickness h of the individual injections is less than 20 m, new injections are emplaced in the middle of the older one (Fig. 13b), until the total thickness reaches 20 m. As the reaction rims of hornblende phenocrysts (Fig. 6c) are thin (less than 60 μm), we can consider that ascent of magma from the source region was very fast (less than 25 days?) (Rutherford and Hill, 1993). In our numerical model, each injection is consequently emplaced instantaneously. Thickness and time between injections are constant from the beginning to the end of pluton emplacement.

6.2.3. Results

6.2.3.1. Maximum duration of BMp emplacement.

The first goal of our numerical simulation was to find an estimate of the maximum duration of the BMp construction. We chose to approach this problem by taking various thicknesses of individual injections (h), and finding for

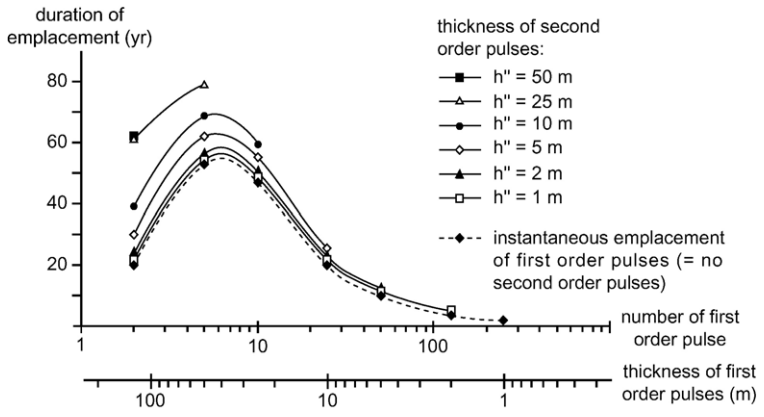

Fig. 14. Maximum duration of the emplacement; for each simulation, the magmatic body is built by successive injections, separated by the maximum time for which there is still melt in the feeder zone. Each point corresponds to the sum of the total inter-pulse time plus the injection time. For the curve labelled 'instantaneous', injections are instantaneously emplaced. In the other curves, injections are built by the accumulation of thinner pulses at a rate constrain by the *magmatic contact criterion*. The thickness of these second order pulses (h'') is noted in the legend.

each thickness the critical time between injections $t_{i\ cr.}$, which is defined as the maximum time between two successive injections for which there is still melt in the contact zone between the pulses. In this case, the next injection is emplaced into unsolidified material, which does not create solid-state deformation or chilled margin between the two pulses. We call this scenario the *magmatic contact criterion*. As $t_{i\ cr}$ will necessarily increase from the beginning to the end of pluton emplacement, it is sufficient to check the temperature at the contact between the two first injections, which will be compatible with the absence of chilled margins if higher than the solidus temperature. Fig. 14 shows the results of the different simulations. *The magmatic contact criterion* suggests that the maximum duration of the BMp construction depends primarily on the thickness or number of individual pulses: we find a maximum duration of around 55 years for thickness of pulses between 30 and 50 m (Fig. 14, instantaneous curve). The maximum duration decreases for thinner and thicker pulses, and is very short (<5 years) for a great number of thin pulses. These durations, which are obtained assuming an instantaneous injection of individual pulses, correspond to the total inter-pulse time. To specify our results, we envisage that each pulse is not injected instantaneously but is built by accumulation of thinner "second order" pulses at a rate constrained by $t_{i\ cr}$, that we found when we injected magma instantaneously. The maximum duration of the emplacement of the BMp is then between 50 and 80 years, depending on the size of these second order pulses (noted h'' in Fig. 14).

6.2.3.2. Effects of interval time and intrusion thickness.
To examine the respective influence of the time between successive injections and injection thickness, we fixed the thickness of the injections h and varied the time interval t_i, allowing the temperature evolution at the lower and the upper contacts to be estimated (Fig. 15). Fig. 15a and c represents the results for h equal to 25 m, and varied t_i. Fig. 15b and d shows the results for t_i equal to 5 yrs and varied h. All the other simulations with different fixed h or fixed t_i show the same general trend. Results for the maximum temperature reached at the contacts and the duration of the thermal perturbation are summarized in Appendix Table 3. We note the following about the thermal evolution of the lower and upper contacts of the intrusion:

(1) Due to its proximity and constant distance to the injection zone, the temperature at the lower contact shows a characteristic saw-tooth evolution with decreasing amplitude with time. The maximum temperature T_{max} at the lower contact, which could be above the solidus (between 500 and 800 °C), is always attained just at the end of the pluton construction, and decreases with increasing injection thickness and/or time interval. The maximum T_{max} and the maximum duration of the thermal perturbation were attained for a ratio h / t_i between 0.5 and 1 m/yr, which is outside the field of the *magmatic contact criterion* for a constant growth rate (see above). T_{max} is itself a maximum for h=10 m and t_i=10 yrs, which constitutes the parameters for a maximum heating of wallrocks. At a given injection thickness, rocks at the lower contact will be less heated with either a short time interval between injections (<5 yr), or a very long one (>100 yr), but in the latter case, the *magmatic contact criterion* will not be satisfied. Conversely, at a given time interval, rocks at the lower contact will then be less heated with either thin (<2 m) or thick (>50 m) injections.
(2) The upper contact temperature shows a smoother trend due to the buffering effect caused by its increasing distance to the injection site. T_{max} is below 700 °C, is always recorded during the first injection, and is significantly lower than at the lower contact (difference of 200 °C in the 25 m case). After the first injection, the temperature at the contact is significantly lower for long time intervals between pulses than for short, and this effect is more pronounced for thin individual injections. Depending on the time interval, a second peak temperature is observed after the end of emplacement due to the heat released by the cooling pluton below the contact. At a given pulse thickness, T_{max} is greater for short time intervals, and conversely, at a given time interval, T_{max} is greater for thick pulses. The duration of the thermal perturbation follows a similar evolution.

To summarize, the thermal effects at the contacts of the pluton (value of T_{max} and duration of the thermal perturbation) are minimized if the ratio h / t_i is outside the range of 0.5–1, and if the time interval is not too short (i.e. above one week) and the pulses not too thick (i.e. below 100 m). If we combine these results with those about the *magmatic contact criterion*, we can propose that the BMp emplacement could have involved a combination of pulse thickness and time interval between pulses as outlined in Fig. 16. Optimal configurations are constituted by pulse thickness in the order of 10–80 m, emplaced at a time interval between one week and one year.

6.2.4. Internal structure and thermal simulation
The thermal modelling outlined above relies on several criteria that must be correct for results to be applicable.

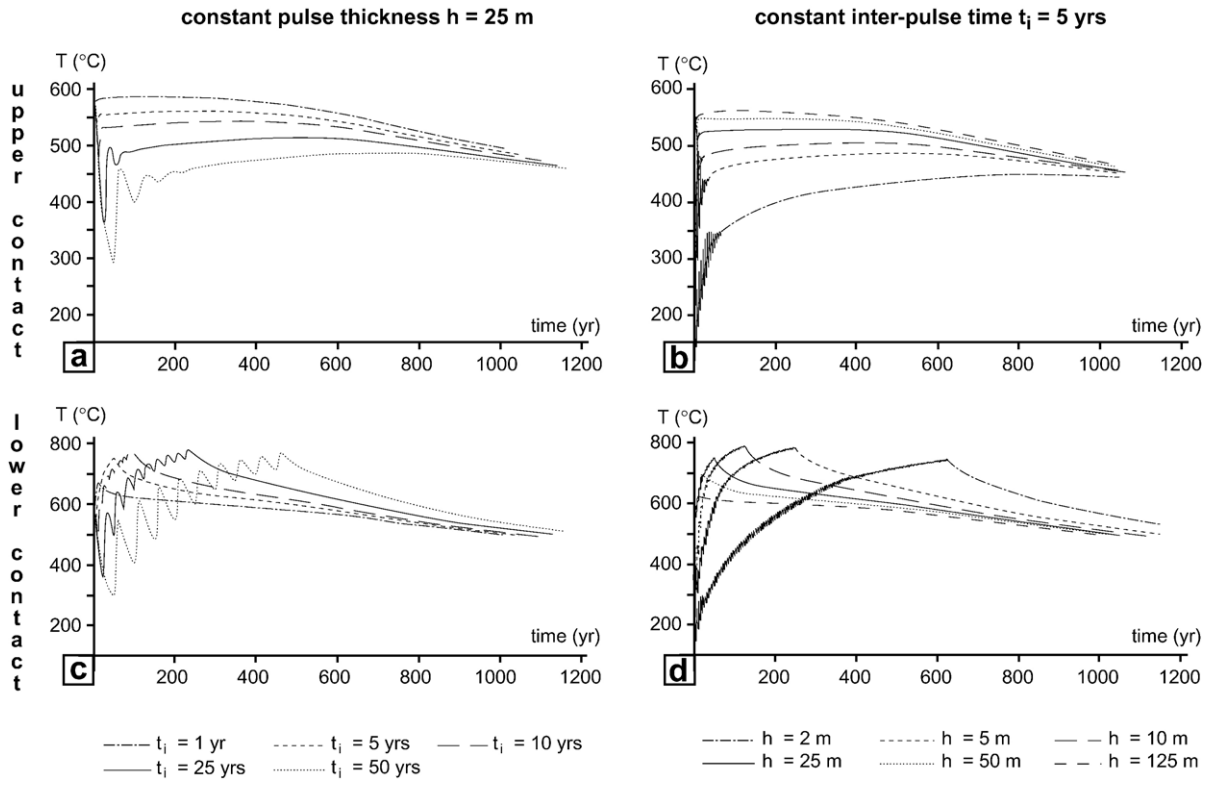

Fig. 15. Evolution of the temperature at the lower (c and d) and upper (a and b) contacts of the intrusion from the first injection until the contact cooled under 500 °C; for different values of t_h and t_i; a and c) the thickness of the injections is fixed and the time between them varies from 1 to 100 years; b and d) the time between injections is fixed and their thickness varies from 5 to 125 m. See text for discussion.

Below we review these criteria and the data that led us to make them. The strongest criterion we have used to constrain the maximum duration of BMp construction is the so-called *magmatic contact criterion*, i.e. the absence of chilled margins at internal contacts. We hypothesize that this observation supports our interpretation of the presence of a permanent magma chamber during pluton emplacement. A permanent magma chamber is not synonymous with a large reservoir of magma at any one instant. Rather, it merely means that the overlying sheet was at or near its solidus during intrusion of the next sheet (T at its base $\geq T_{\text{solidus}}$). If this criterion is satisfied, then the pluton texture could be homogeneous, as observed in the field. The validity of this criterion depends on how we are able to interpret this kind of texture. Moreover, one type of texture could be produced by several different scenarios, and we can imagine more complicated histories. For example, resorbtion or recrystallization at the internal contacts could occur, which could have resulted in the same texture but does not allow us to provide any time constraints. But these scenarios would imply the full crystallization of a pulse before the intrusion of the next one, and then an indeterminable time gap between two successive pulses. Thus, if the pluton consists of sheets, our time estimate is a minimum. We hypothesize, however, that our assumption of intrusion of the new pulse at the base of a non-fully crystallized one is valid. Observations that support this interpretation are, among others, the simple 3D geometry, the homogeneity of the internal structure, the absence of any solid-state deformation in the pluton except at the contact, and the remarkable homogeneity of the rock composition, which argues for a short elapsed time between source extraction of the earliest and latest magmas.

A limitation of our model is the instantaneous injection of individual magma pulses, as the injections occur in one time-step of the numerical simulation. To test the validity of this assumption, we can calculate an instantaneous magma supply rate by dividing the volume of each injection by the time-step. This instantaneous filling rate must be equal to the volumetric flow rate in the feeder. Using the formula of the flow rate in a dike as a function of its width (Petford et al., 1993; Cruden, 1998), we can estimate the size of the feeder dike required to feed the pluton at the rate sufficient to satisfy the constraints imposed by our model. Assuming

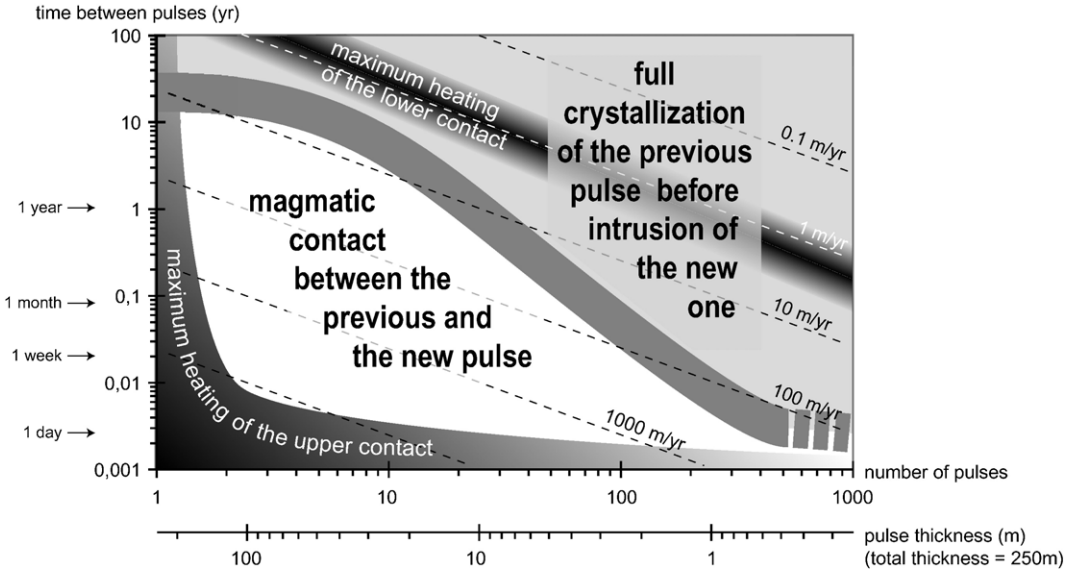

Fig. 16. Summary of the thermal constraints obtained by the numerical simulations; the grey thick line in the middle of the diagram separate an upper zone where plutons with chilled margins are built (*magmatic contact criterion* not satisfied), that is with full crystallization of a pulse before intrusion of the next one, and a lower zone where a permanent magma chamber is maintained in the feeder zone (*magmatic contact criterion* satisfied). Dashed lines outline different rates of vertical uplift of the roof. The two dark grey zones mark the parts of the diagram where the lower or the upper contacts suffer the maximum heating (intensity and duration) (see Table 2). To respect the textural field constraints, BMp emplacement can be modelled by simulations within the permanent magma chamber zone, and as far as possible from the zones where contacts are warmed up.

a length of 1–1.5 km, a density contrast of 0.1, and a magma viscosity of 10^6 Pa.s, the width of the feeding dike is between 2 and 12 m, when thickness of injections are between 1 and 125 m. This width range is compatible with observations of other plutons' feeder zones in the Henry Mountains and other dikes in the vicinity of the BMp.

Another limitation is the constant growth rate assumed from the beginning to the end of the BMp emplacement, even if the growth is discontinuous. The two major structural phases (sheeted growth and fault-assisted growth) may have two different emplacement rates as they correspond to different mechanisms. When growth is accommodated by the movement along faults, there is solely the lithostatic load acting against the supply of the intrusion (there is no elastic flexure or internal cohesion of the host rock). But as the basic emplacement mechanism is the amalgamation of individual pulses, a more or less constant growth rate is compatible with our geologic emplacement model. The wallrocks were bent only at the tip of the laterally propagating first pulse, and this bending is accommodated by both flexure and small-scale fracturing and rotation of the wallrocks. During the intrusion of the following pulses, the roof wallrocks are only vertically displaced, and this movement is accommodated by small-scale fracturing and rotation but only of the margin wallrocks. The initiation of the bysmalith stage occurs when the mechanical continuity of the margin wallrocks can no longer be maintained. Consequently, the bysmalith stage does not necessarily correspond to an increase in the magma supply rate, but may rather be the result of a greater net amount of magma.

If we compare our results to those of Petford and Gallagher (2001) who have numerically simulated the partial melting of the lower crust by periodic intrusion of basalts, we note that their line of maximum heating efficiency, i.e. the balance between heat supply and heat loss ($R=\tau_1/\tau_d=1$; τ_1 is the time between intrusions and τ_d is the characteristic timescale for diffusive heat loss), does not exactly match our results. In our simulations, optimal heating of wallrocks occurs for an intrusion rate around 1 m per year, which corresponds to R between 0.32 and 32 for the studied time intervals and thickness. The reasons for this difference could be: (1) the emplacement of the BMp by under-accretion, which is imposed by the structural constraints on both pluton and wallrocks, versus over-accretion in the case of Petford and Gallagher (2001), (2) the 10 m thick screen of diorite between wallrocks and the new injection at the base of the growing pluton, and (3) the differences between the thermal characteristics of the lithologies in the two models.

6.3. Comparison with other "bysmaliths" in the Henry Mountains

Several intrusions in the Henry Mountains have geometries similar to the BMp, most notably Table Mountain and Bull Mountain on the northernmost intrusive centre in the range, Mt Ellen. Preliminary work suggests, that these cylindrical intrusions both have wallrock orientations and magmatic fabric patterns broadly similar to those observed on the BMp. These intrusions have not yet been studied in detail, so we cannot conclusively demonstrate similarities or differences in emplacement processes with the BMp. However, the similarities suggest that the processes leading to formation of the BMp may have been active throughout the region.

These intrusions are of particular interest because they appear to record evolution of emplacement mechanism during the pluton history. The factors controlling the change from sill-like emplacement to bysmalith-like emplacement are unknown. Our observations contradict Pollard and Johnson's (1973) suggestion that the switch occurs once a laccolith reaches a particular radius relative to its thickness. Other possible controlling factors may be wallrock lithology, variations in feeder position or geometry, etc. Further study may help to resolve these questions.

6.4. Comparison with fossil and actual volcanic and plutonic arc systems

One way to evaluate the extremely rapid rate of emplacement we have obtained is to compare our results with other fossil and actual natural magmatic systems. Magma production rates can be estimated from volcanic output rates and assumptions about the ratio of intrusive to extrusive products (Crisp, 1984; Shaw, 1985). Volcanic output rates are typically in the range of 10^{-2} to 10^{-4} km^3/yr (Shaw, 1985) and a ratio of intrusive to extrusive volumes of around 2–5 can be assumed for tabular intrusions (Annen and Sparks, 2002). The maximum duration of emplacement we have obtained yields an averaged emplacement rate around 10^{-3} km^3/yr, which is clearly comparable with volcanic data. A better understanding of emplacement mechanisms (timescale, continuous versus discontinuous) of these kinds of intrusions will come from detailed observations of changes in vertical elevation in active magmatic zones (Berrino, 1998; Nakada and Motomura, 1999; Karner et al., 2001; Barmin et al., 2002). Vertical topographic elevation changes as large as 100 m/yr due to the growth of an underlying magmatic intrusion have already been observed (Minakami et al., 1951). Vertical *magmatic* uplift of up to 5 cm/yr are measured in the Andes by GPS and radar interferometry (Pritchard and Simons, 2002; Bonvalot et al., 2005), and this uplift is not systematically associated with volcanic activity, and could then be associated to *plutonic* activity. Although we do not know the exact depth and shape of the growing magmatic body in these examples, which is modelled between 5 and 15 km by these authors. These results clearly demonstrate that plutons can be emplaced extremely rapidly in the shallow crust, and that the rates of plutonic and volcanic processes could be similar, a result which is of great importance for the general knowledge and interpretation of magma transfer in arc systems.

Concerning the temporal evolution of the emplacement rates of magmatic bodies, pulses at many different timescales can be identified. There are magmatic bodies constructed by batches which are separated by million of years (e.g. Paquette et al., 2003). This is characteristic of nested bodies such as the Tuolumne Intrusive Suite (Bateman and Chappell, 1979; Coleman et al., 2004). Note that within one main emplacement episode, short-lived events (50 000 yrs) of higher activity may exist (Saint-Blanquat et al., 1998, 2001). Fialko and Simons (2001) evoked temporal evolution of the Socorro magma body on a timescale of a few tens of years. To fit our petrostructural constraints, the BMp could, for example, have been constructed by pulses of 20 m thickness every 6 months. As rates of emplacement seem to be independent of tectonic context (St-Blanquat et al., submitted), mechanisms might be hidden in the source region (Petford and Gallagher, 2001; Annen et al., 2006) or during ascent (Olsen and Christensen, 1986; Rabinowicz et al., 2001).

7. Conclusions

A new study of the 3D geometry, composition, internal structure, and microstructures of the Black Mesa pluton allow us to propose an original emplacement model. Our data show that the emplacement of this small pluton (about 0.5 km^3) occurred by the vertical stacking of individual magma pulses accreted from below (under-accretion). Textural analysis permits us to propose that a molten zone was maintained at the base of the growing pluton during its growth. We have found remnants of each stage of pluton emplacement and we propose a kinematic interpretation to explain fabric orientation and intensity. Our data show that the internal structure of the pluton, and particularly the lineations, has recorded an evolving pluton emplacement process that consisted of three mechanisms: (1) initial intrusion

of a sill by horizontal lateral propagation at a weak interface, the Summerville Fm., between two rigid layers of sandstones, the Entrada Fm. below and the Morisson Fm. above; (2) formation of a sheeted body by vertical growth accommodated mainly by small-scale faulting and rotation of wallrocks at the western part of the pluton, and by vertical lifting of roof wallrocks along peripheral faults at its eastern part; (3) late intrusion of minor dikes, which cross-cuts all the previous structures.

These structural results have been used to constrain the duration and rate of the BMp construction, by using a 1D thermal numerical simulation to model the evolution of the temperature in the growing pluton and its wallrocks for different emplacement scenarios. The two characteristic parameters used to constrain the time and rate of emplacement are the time between each injection (or frequency of pulse intrusion) and the thickness of each injection (equivalent to the number of pulses). The results were obtained by comparing the modelled temperature profiles with two petrostructural constraints which are: (1) the absence of solid-state textures around internal contacts, which implies that a melted zone was maintained in the intrusion during its emplacement, and (2) the absence of significant contact metamorphism or recrystallization, which means that the increase of temperature in the host rock was relatively small, or short-lived, or both. We propose that the emplacement of the BMp was a geologically instantaneous event, with a maximum duration on the order of 100 years, implying minimum averaged vertical displacement rates of the topography above the pluton greater than 2 m per year. This is a mean rate, but emplacement could have been achieved by an alternation of periods of low inflation rates followed by period of very fast inflation rates of the topographic surface (in the order of 20 m/yr). These very fast rates of magma intrusion and topographic elevation are compatible with observed actual volcanic systems. Additional detailed studies of these systems would yield further constraints and understanding of subvolcanic bodies such as the Black Mesa pluton. Finally, our data show that the rates of plutonic and volcanic processes may be similar, a result of great importance for the general knowledge and interpretation of magma transfer in arc systems.

Acknowledgements

Field work was funded by C.N.R.S./N.S.F. grant no. 12971, and National Science Foundation grant EAR-0003574. Lab work was supported by the LMTG, except for image analysis which was conducted at the Laboratoire de Planétologie et Géodynamique of Nantes University (France). We thank K. Charkoudian for her help during fieldwork. R. Peyron, F. de Parseval, and C. Cavaré-Hester are thanked for thin section preparation and drafting respectively. Comments on drafts of the manuscript by C. Annen and Ph. Olivier, and constructive reviews by J.M. Tubia, A.R. Cruden, and N. Petford are acknowledged. Stimulating remarks by the Editor Jean-Pierre Burg were sincerely appreciated.

Appendix A

Appendix Table 1
Whole rock chemical analysis of six samples from the Black Mesa pluton. Analyses by ICPMS at the SARM, Nancy; major elements in wt.%, trace elements in ppm

Sample	BM 40	BM 37	BM 33	BM 04	BM 64	BM 18	Average	σ
Elevation (m)	1707	1722	1807	1829	1871	1893		
SiO2	60.17	59.47	60.21	59.92	59.74	60.24	59.96	0.31
Al2O3	18.83	18.62	18.63	18.62	18.57	18.76	18.67	0.10
Fe2O3tot	5.38	5.10	5.02	5.14	4.94	5.10	5.11	0.15
MnO	0.16	0.16	0.16	0.17	0.13	0.12	0.15	0.02
MgO	1.52	1.53	1.53	1.43	1.35	1.51	1.48	0.07
CaO	6.29	6.52	6.28	5.99	5.49	5.37	5.99	0.47
Na2O	4.51	4.63	4.46	4.56	4.54	4.82	4.59	0.13
K2O	2.09	2.09	2.17	2.17	2.46	2.46	2.24	0.17
TiO2	0.58	0.56	0.56	0.56	0.55	0.57	0.56	0.01
P2O5	0.23	0.24	0.25	0.23	0.23	0.26	0.24	0.01
PF	0.47	1.03	0.69	1.11	0.89	1.02	0.87	0.24
Total	100.23	99.95	99.96	99.90	98.89	100.23		
As	1.7	3.0	1.9	2.9	3.4	4.2	2.8	0.9
Ba	970.4	853.7	923.8	911.2	997.5	1006.0	943.8	58.4
Bi	0.1	0.1	0.1	0.1	0.2	0.1	0.1	0.1
Ce	76.8	79.2	79.4	73.8	79.5	82.1	78.5	2.8
Co	6.8	6.3	6.1	6.5	6.4	6.0	6.4	0.3
Cs	0.9	0.8	1.5	1.1	1.1	2.3	1.3	0.6
Cu	11.6	5.8	6.4	5.7	9.1	5.8	7.4	2.4
Dy	4.6	4.6	4.5	4.4	4.6	4.6	4.5	0.1
Er	2.6	2.7	2.7	2.5	2.5	2.6	2.6	0.1
Eu	2.0	2.0	2.0	1.9	2.0	2.1	2.0	0.1
Ga	22.3	22.0	21.7	21.7	22.0	21.9	21.9	0.2
Gd	5.4	5.4	5.4	5.2	5.5	5.6	5.4	0.1
Hf	4.4	4.2	4.3	4.1	4.3	4.4	4.3	0.1
La	37.5	38.6	38.5	35.6	38.8	40.0	38.2	1.5
Nb	6.1	6.2	6.4	6.2	6.3	6.5	6.3	0.1
Nd	36.3	37.3	37.6	35.3	37.3	38.8	37.1	1.2
Pb	15.5	13.8	12.3	13.1	9.3	13.6	12.9	2.1
Pr	9.4	9.6	9.7	9.1	9.7	10.0	9.6	0.3
Rb	30.9	31.8	35.1	32.1	39.8	40.6	35.1	4.3
Sm	6.9	6.9	7.0	6.6	6.9	7.1	6.9	0.2
Sn	1.2	1.1	1.2	1.0	1.2	1.2	1.1	0.1
Sr	926.5	886.1	877.7	853.6	814.1	783.3	856.9	51.7
Th	6.4	6.5	6.4	6.1	6.4	6.8	6.4	0.2
U	1.8	1.8	1.8	1.6	1.8	1.9	1.8	0.1
V	69.3	65.8	64.1	66.1	64.2	66.0	65.9	1.9
Y	25.3	25.7	25.9	24.7	25.8	26.3	25.6	0.6
Yb	2.7	2.7	2.8	2.6	2.7	2.8	2.7	0.1
Zn	86.3	124.0	90.8	78.9	71.1	64.5	85.9	21.0
Zr	177.4	172.3	175.0	167.2	179.0	178.8	175.0	4.6

Appendix Table 2
Raw AMS data. Measurements with an Agico KLY-3; averaging by a tensor method, following Jelinek (1981)

Site	*x*	*y*	Km	σKm	Kmax	Kmax*D*	Kmax*I*	Kint	Kint*D*	Kint*I*	Kmin	Kmin*D*	Kmin*I*	Foliation			Pp%	Lp%	Fp%	*T*
BM002	534,334	4,196,512	19,612	2364	19,700	288	41	19,626	140	44	19,509	33	16	123	S	74	0.98	0.38	0.60	0.23
BM004	534,714	4,196,112	31,740	417	32,013	101	37	31,688	194	4	31,518	289	52	19	E	38	1.57	1.02	0.54	−0.31
BM005	534,692	4,196,005	35,227	461	35,514	170	73	35,267	65	5	34,899	334	17	64	S	73	1.76	0.70	1.05	0.20
BM006	534,755	4,195,994	28,346	1773	28,599	69	7	28,298	322	67	28,140	162	22	72	N	68	1.63	1.06	0.56	−0.31
BM011	534,186	4,196,100	26,729	1817	26,879	276	4	26,720	183	30	26,588	13	59	103	S	31	1.09	0.59	0.50	−0.09
BM012	534,057	4,195,894	10,955	972	11,029	279	15	10,992	28	50	10,843	178	36	88	N	54	1.71	0.33	1.37	0.61
BM013	533,932	4,195,811	12,038	118	12,119	70	58	12,061	233	30	11,934	327	8	57	S	82	1.55	0.48	1.07	0.38
BM014	534,091	4,195,776	10,856	398	10,974	75	33	10,850	259	57	10,743	166	2	76	N	88	2.15	1.15	0.99	−0.07
BM015	534,229	4,195,765	8132	384	8251	181	20	8127	327	66	8017	86	12	176	W	78	2.91	1.52	1.37	−0.05
BM016	534,395	4,196,108	21,356	2137	21,740	116	1	21,304	207	65	21,022	26	25	116	S	65	3.41	2.04	1.34	−0.21
BM017	534,595	4,196,211	31,240	1000	31,395	177	20	31,286	81	18	31,040	312	63	42	E	27	1.14	0.35	0.79	0.39
BM018	534,751	4,196,193	27,453	1448	27,625	83	10	27,491	178	28	27,243	336	60	66	S	30	1.40	0.49	0.91	0.30
BM019	535,009	4,196,305	32,014	646	32,294	107	20	32,157	200	6	31,592	305	69	35	E	21	2.22	0.43	1.79	0.61
BM020	534,939	4,196,451	29,169	1899	29,474	88	2	29,102	178	12	28,931	350	78	80	S	12	1.87	1.28	0.59	−0.37
BM021	535,232	4,196,627	29,218	1667	29,424	39	18	29,353	133	12	28,878	254	68	164	E	22	1.89	0.24	1.64	0.74
BM022	534,009	4,196,223	17,975	2155	18,108	122	75	18,036	331	13	17,781	239	7	149	E	83	1.84	0.40	1.43	0.56
BM024	533,954	4,196,317	13,066	976	13,149	322	2	13,086	70	84	12,962	232	6	142	E	84	1.44	0.48	0.95	0.33
BM025	533,842	4,196,331	20,849	79	20,939	144	53	20,851	11	27	20,757	269	23	179	E	67	0.88	0.42	0.46	0.04
BM026	533,870	4,196,512	31,198	3107	31,460	82	60	31,191	183	6	30,943	277	29	7	E	61	1.67	0.86	0.80	−0.04
BM027	534,340	4,197,398	16,261	7749	16,304	353	39	16,276	256	9	16,201	155	50	65	N	40	0.64	0.17	0.46	0.46
BM028	534,346	4,197,523	38,213	2079	38,384	68	31	38,343	329	14	37,911	218	55	128	N	35	1.25	0.11	1.14	0.82
BM030	534,737	4,196,057	33,811	1306	34,131	93	16	33,786	2	3	33,515	263	73	173	E	17	1.84	1.02	0.81	−0.12
BM031	534,739	4,196,050	32,335	3896	32,680	86	67	32,317	243	21	32,007	337	8	67	S	82	2.10	1.12	0.97	−0.07
BM032	534,741	4,196,044	35,604	1774	35,831	299	19	35,638	86	67	35,343	205	12	115	N	78	1.38	0.54	0.83	0.21
BM033	535,238	4,196,622	37,581	465	37,900	214	25	37,610	311	15	37,234	68	60	158	W	30	1.79	0.77	1.01	0.13
BM034	535,241	4,196,619	33,852	3401	34,120	39	27	34,010	140	21	33,426	263	55	173	E	35	2.08	0.32	1.75	0.68
BM035	535,247	4,196,615	31,721	182	31,901	350	1	31,745	260	1	31,519	136	89	46	N	1	1.21	0.49	0.72	0.19
BM037	534,683	4,197,523	47,815	4297	50,052	351	35	47,645	82	1	45,749	173	55	83	N	35	9.40	5.05	4.14	−0.10
BM039	534,954	4,197,446	45,694	5038	46,180	338	41	45,755	81	15	45,147	186	46	96	N	44	2.29	0.93	1.35	0.18
BM040	535,129	4,197,237	52,644	1598	53,079	346	17	52,773	79	9	52,080	195	71	105	N	19	1.92	0.58	1.33	0.39
BM043	535,020	4,196,143	30,427	4695	30,590	61	68	30,472	300	12	30,217	206	18	116	N	72	1.23	0.39	0.84	0.37
BM046	533,888	4,196,529	24,204	1885	24,367	52	57	24,228	218	32	24,016	312	6	42	E	84	1.46	0.57	0.88	0.21
BM047	533,892	4,196,566	30,870	523	31,119	116	36	30,941	13	17	30,551	263	49	173	E	41	1.86	0.57	1.27	0.38
BM049	533,587	4,196,744	38,574	949	38,985	338	12	38,569	247	4	38,169	138	77	48	N	13	2.14	1.08	1.05	−0.01
BM050	533,642	4,196,671	42,694	1456	42,969	25	34	42,620	122	9	42,491	225	54	135	E	36	1.12	0.82	0.30	−0.46
BM053	535,145	4,196,354	40,105	2029	40,401	336	75	40,120	194	12	39,794	103	9	13	W	81	1.52	0.70	0.82	0.08
BM054	535,364	4,196,601	28,577	835	29,084	350	34	28,755	226	40	27,893	104	32	14	W	58	4.27	1.14	3.09	0.46
BM055	535,579	4,196,734	35,077	857	35,324	100	25	35,155	197	15	34,752	316	60	46	S	30	1.65	0.48	1.16	0.41
BM056	535,258	4,196,944	36,983	608	37,246	343	42	36,989	91	19	36,714	199	42	109	N	48	1.45	0.69	0.75	0.04
BM060	534,100	4,197,215	33,441	820	33,723	13	33	33,424	115	18	33,177	228	51	138	E	39	1.64	0.89	0.74	−0.09
BM061	533,850	4,196,868	36,795	1582	37,070	55	16	36,707	323	5	36,609	216	74	126	N	16	1.26	0.99	0.27	−0.57
BM064	534,945	4,196,699	28,848	1108	29,104	302	42	28,725	151	44	28,716	46	15	136	W	75	1.35	1.32	0.03	−0.96

(*continued on next page*)

Appendix Table 2 (*continued*)

Site	*x*	*y*	Km	σKm	Kmax	Kmax*D*	Kmax*I*	Kint	Kint*D*	Kint*I*	Kmin	Kmin*D*	Kmin*I*	Foliation			Pp%	Lp%	Fp%	*T*
BM065	535,150	4,196,921	21,562	1669	21,681	322	59	21,579	138	31	21,425	229	2	139	E	88	1.19	0.47	0.72	0.21
BM066	534,961	4,197,050	28,853	1602	29,103	105	11	28,930	10	23	28,527	219	64	129	N	26	2.02	0.60	1.41	0.40
BM067	535,005	4,197,216	22,453	593	22,796	315	3	22,405	49	47	22,158	222	43	132	N	47	2.88	1.74	1.11	−0.22
BM068	534,796	4,197,273	13,080	3412	13,141	86	12	13,086	351	22	13,013	202	64	112	N	26	0.98	0.42	0.56	0.14
BM069	534,519	4,197,342	27,437	3551	27,626	77	25	27,467	325	39	27,217	191	41	101	N	49	1.50	0.58	0.92	0.23
BM100	534,711	4,196,103	36,997	1075	37,204	145	26	37,059	238	8	36,727	344	63	74	S	27	1.30	0.39	0.91	0.40
BM101	534,713	4,196,082	35,924	1225	36,119	99	3	36,012	191	36	35,641	5	54	95	S	36	1.34	0.30	1.04	0.56
BM102	534,654	4,196,495	36,767	616	36,927	54	20	36,855	321	7	36,521	213	69	123	N	21	1.11	0.20	0.91	0.65
min			8132	79	8251		1	8127		1	8017		2				0.64	0.11	0.03	−0.96
max			52,644	7749	53,079		75	52,773		84	52,080		89				9.40	5.05	4.14	0.82
mean			29,447	1734	29,717		30	29,470		25	29,156		42				1.85	0.79	1.04	0.16
σ			9887	1484	10,036		21	9892		21	9740		25				1.27	0.74	0.66	0.36

x and *y* UTM coordinates in meters; susceptibilities in 10-6 SI.

Appendix Table 3
Maximum temperature and duration of the thermal anomaly (time during which the contact remains at temperature above 500 °C) at the lower and upper contacts for the different simulations

	T_{max} at the upper contact (°C)/time above 500 °C (yr)											
Inter-pulse time (yrs)	Pulse thickness (m)											
	2		5		10		25		50		125	
	T_{max}	Δ*t*>500 °C	T_{max}	Δ*t*>500 °C	T_{max}	Δ*t*>500 °C	T_{max}	Δ*t*>500 °C	T_{max}	Δ*t*>500 °C	T_{max}	Δ*t*>500 °C
1	536	851	671	921	599	944	587	973	593	987	596	994
5	476		513	601	564	837	575	918	585	955	594	985
10	438		486		527	527	572	871	585	929	593	976
25	378		437		475		556	630	585	875	593	956
50			392		436		487		585	768	593	935
100					392		479		583	37	593	901
	T_{max} at the lower contact (°C)/time above 500 °C (yr)											
1	790	1085	765	1046	741	1025	672	1010	617	1001	597	996
5	746	1186	784	1117	792	1079	753	1042	699	1017	623	1001
10	669	1163	760	1152	791	1113	772	1069	725	1034	643	1005
25	524	79	681	1144	759	1169	780	1113	751	1069	669	1016
50			564	616	693	1128	767	1134	760	1116	686	1031
100					573	559	728	1134	752	1205	699	1056

See text for discussion.

References

Acocella, V., 2000. Space accommodation by roof lifting during pluton emplacement at Amiata (Italy). Terra Nova 12, 149–155.

Annen, C., Sparks, R.S.J., 2002. Effects of repetitive emplacement of basaltic intrusions on thermal evolution and melt generation in the crust. Earth and Planetary Science Letters 203, 937–955.

Annen, C., Blundy, J.D., Sparks, R.S.J., 2006. The genesis of calcalkaline intermediate and silicic magmas in deep crustal hot zones. Journal of Petrology 47, 505–539.

Armstrong, R.L., Ward, P., 1991. Evolving geographic pattern of Cenozoic magmatism in the North American Cordillera: the temporal and spatial association of magmatism and metamorphic core complexes. Journal of Geophysical Research 96, 13,201–13,224.

Barmin, A., Melnik, O., Sparks, R.S.J., 2002. Periodic behavior in lava dome eruptions. Earth and Planetary Science Letters 199, 173–184.

Barros, C.E.M., Barbey, P., Boullier, A.M., 2001. Role of magma pressure, tectonic stress and crystallization progress in the emplacement of syntectonic granites. The A-type Estrela granite complex (Carajas Mineral Province, Brazil). Tectonophysics 343, 93–109.

Bateman, P.C., Chappell, B.W., 1979. Crystallization, fractionation, and solidification of the Tuolumne Intrusive series, Yosemite National Park, California. Geological Society of America Bulletin 90, 465–482.

Bergerat, F., Bouroz-Weil, C., Angelier, J., 1992. Paleostresses inferred from macrofractures, Colorado Plateau, western U.S.A. Tectonophysics 206, 219–243.

Berrino, G., 1998. Detection of vertical ground movements by sea-level changes in the Neapolitan volcanoes. Tectonophysics 294, 323–332.

Bonvalot, S., Froger, J.L., Remy, D., Bataille, K., Cayol, V., Clavero, J., Comte, D., Gabalda, G., Gonzales, K., Lara, L., Legrand, D., Macedo, O., Naranjo, J., Mothes, P., Pavez, A. Robin, C., 2005. Applications of INSAR interferometry and geodetic surveys for monitoring Andean volcanic activity: first results from ASAR-ENVISAT data. 6th International Symposium on Andean Geodynamics, Barcelona.

Borradaile, G.J., Puumala, M., Stupavsky, M., 1991. Anisotropy of complex magnetic susceptibility as an indicator of strain and petrofabric in rocks bearing sulphides. Tectonophysics 202, 309–318.

Bourroz, C., Bergerat, F., Angelier, J., 1989. From distribution of joint patterns in monoclinal flexures to tectonic chronology : examples in the Colorado Plateau (Utah–Arizona–New-Mexico, U.S.A.). Geodinamica Acta 3 (4), 305–318.

Clark, D.A., 1997. Magnetic petrophysics and magnetic petrology: aids to geological interpretation of magnetic surveys. AGSO Journal of Australian Geology and Geophysics 17 (2), 83–103.

Coleman, D.S., Gray, W., Glazner, A.F., 2004. Rethinking the emplacement and evolution of zoned plutons: geochronologic evidence for incremental assembly of the Tuolumne Intrusive Suite, California. Geology 32 (5), 433–436.

Corry, C.E., 1988. Laccoliths, mechanics of emplacement and growth. Special Paper - Geological Society of America 220 110 pp.

Coulson, I.M., Villeneuve, M.E., Dipple, G.M., Duncan, R.A., Russell, J.K., Mortensen, J.K., 2002. Time-scales of assembly and thermal history of a composite felsic pluton : constraints from the Emerald Lake area, northern Canadian Cordillera, Yukon. Journal of Volcanology and Geothermal Research 114, 331–356.

Crisp, J.A., 1984. Rate of magma emplacements and volcanic output. Journal of Volcanic and Geothermal Research 20, 177–211.

Cruden, A.R., 1998. On the emplacement of tabular granites. Journal of the Geological Society of London 155, 853–862.

Cruden, A.R., Mc Caffrey, K.J.W., 2001. Growth of plutons by floor subsidence: implications for rates of emplacement, intrusion spacing and melt-extraction mechanisms. Physics and Chemistry Earth (A), Solid Earth and Geodesy 26, 303–315.

Ellwood, B.B., Whitney, J.A., 1980. Magnetic fabric of the Elberton granite, northeast Georgia. Journal of Geophysical Research 85, 1481–1486.

Engel, C., 1959. Igneous rocks and constituent hornblends of the Henry mountains, Utah. Geological Society of America Bulletin 70, 971–980.

Fialko, Y., Simons, M., 2001. Evidence for on-going inflation of the Socorro magma body, New Mexico, from Interferometric Synthetic Aperture Radar imaging. Geophysical Research Letters 28, 3549–3552.

Frost, B.R., Lindsley, D.H., 1991. Occurrence of iron–titanium oxides in igneous rocks. Reviews in Mineralogy 25, 433–468.

Frost, B.R., Lindsley, D.H., Andersen, D.J., 1988. Fe–Ti oxide–silicate equilibria; assemblages with fayalitic olivine. American Mineralogist 73, 727–740.

Furlong, K.P., Hanson, R.B., Bowers, J.R., 1991. Modeling thermal regimes. Reviews in Mineralogy 26, 437–498.

Gaillot, P., de Saint-Blanquat, M., Bouchez, J.L., 2006. Effects of magnetic interactions in anisotropy of magnetic susceptibility: discussion on models and experiments — implications for the quantification of rock fabrics. Tectonophysics 418 (1–2), 3–19.

Gilbert, G.K. 1877. Report on the Geology of the Henry Mountains. USGS Rocky Mountains Region, 170 pp.

Glazner, A.F., Bartley, J.M., Coleman, D.S., Gray, W., Taylor, R.Z., 2004. Are plutons assembled over millions of years by amalgamation from small magma chambers? GSA Today 14 (4/5), 4–11.

Grégoire, V., de Saint-Blanquat, M., Nédélec, A., Bouchez, J.L., 1995. Shape anisotropy versus magnetic interactions of magnetic grains: experiments and applications to AMS in granite rocks. Geophysical Research Letters 22, 2765–2768.

Gregoire, V., Darrozes, J., Gaillot, P., Nedelec, A., Launeau, P., 1998. Magnetic grain shape fabric and distribution anisotropy vs rock magnetic fabric: a 3D case study. Journal of Structural Geology 20 (7), 937–944.

Gvirtzman, Z., Garfunkel, Z., 1996. Numerical solutions for the one-dimensional heat conduction equation using a spreadsheet. Computers et Geosciences 22, 1147–1158.

Habert, G., de Saint-Blanquat, M., 2004. Rate of construction of the Black Mesa bysmalith, Henry Mountains, Utah. In: Breitkreuz, C., Petford, N. (Eds.), Physical Geology of High-level Magmatic Systems, vol. 234. Geological Society, London, pp. 163–173. Special Publications.

Horsman, E., Tikoff, B., Morgan, S., 2005. Emplacement-related fabric and multiple sheets in the Maiden Creek sill,, Henry Mountains, Utah, USA. Journal of Structural Geology 27 (8), 1426–1444.

Hunt, C.B., Averitt, P., Miller, R.L., 1953. Geology and geography of the Henry mountains region, Utah. USGS professional Paper, 228, 234 pp.

Hutton, D.H.W., 1988. Granite emplacement mechanism and tectonic controls: inferences from deformation studies. Transactions of the Royal Society of Edinburgh: Earth Sciences 79, 245–255.

Ishihara, S., 1977. The magnetite-series and ilmenite series granitic rocks. Mining Geology 27, 293–305.

Jackson, M.D., Pollard, D.D., 1988. The laccolith-stock controversy: new results from the southern Henry mountains, Utah. Geological Society of America Bulletin 100, 117–139.

Jackson, M.D., Noller J.S., 1991. Geologic map of the Copper Creek Benches quadrangle, Garfield county, Utah. Utah Geological and Mineral Survey, Open-file report 209.

Jelinek, V., 1981. Characterization of the magnetic fabrics of rocks. Tectonophysics 79, 63–67.

Johnson, A.M., Pollard, D.D., 1973. Mechanics of growth of some laccolithic intrusions in the Henry Mountains, Utah, I. Tectonophysics 18, 261–309.

Jover, O., Rochette, P., Lorand, J.P., Maeder, M., Bouchez, J.L., 1989. Magnetic mineralogy of some granites from the French Massif Central: origin of their low-field susceptibility. Physics of the Earth and Planetary Interiors 55, 79–92.

Karner, D.B., Marra, F., Florindo, F., Boschi, E., 2001. Pulsed uplift estimated from terrace elevations in the coast of Rome: evidence for a new phase of volcanic activity? Earth and Planetary Science Letters 188, 135–148.

Khan, M.A., 1962. The anisotropy of magnetic susceptibility of some igneous and metamorphic rocks. Journal of Geophysical Research 67 (B7), 2873–2885.

Koch, F.G., Johnson, A.M., Pollard, D.D., 1981. Monoclinal bending of strata over laccolithic intrusions. Tectonophysics 74, T21–T31.

Larson M.J, Bromfield C.S., Dubiel R.F., Patterson C.G., Peterson F., 1985. Geologic map of the Little Rockies wilderness study area and the Mt. Hillers and Mt. Pennell study areas, and vicinity, Garfield County, Utah. U.S. Geological Survey Map MF-1776-B.

Liss, D., Hutton, D.H.W., Owens, W.H., 2002. Ropy flow structures: a neglected indicator of magma flow direction in sills and dikes. Geology 30 (8), 715–718.

Minakami, T., Ishikawa, T., Yagi, K., 1951. The 1944 eruption of volcano Usu in Hokkaido, Japan. Volcanological Bulletin serie 2 (11), 5–157.

Morgan, S.S., Law, R.D., Nyman, M.W., 1998. Laccolith-like emplacement model for the Papoose Flat pluton based on porphyroblast-matrix analysis. Geological Society of America Bulletin 110, 96–110.

Morgan, S., Horsman, E., Tikoff, B., de Saint-Blanquat, M., Habert, G., 2005. Sheet-like emplacement of satellite laccoliths, sills, and bysmaliths of the Henry Mountains, southern Utah. In: Pederson, J., Dehler, C.M. (Eds.), Interior Western United States: Geological Society of America Field Guide 6, pp. 283–309. doi:10.1130/2005.fld006(14).

Nakada, S., Motomura, Y., 1999. Petrology of the 1991–1995 eruption at Unzen: effusion pulsation and groundmass crystallization. Journal of Volcanology and Geothermal Research 89, 173–196.

Nelson, S.T., 1997. Reevaluation of the Central Colorado plateau laccoliths in the light of new age determination. USGS Bullettin 2158, 37–39.

Nelson, S.T., Davidson, J.P., 1993. Interaction between manthe-derived magmas and mafic crust, Henry Mountains, Utah. Journal of Geophysical Research 98 (B2), 1837–1852.

Nelson, S.T., Davidson, J.P., 1997. The petrogenesis of the Colorado plateau laccolith and their relationship to regional magmatism. USGS Bulletin 2158, 85–100.

Nelson, S.T., Davidson, J.P., Sullivan, K.R., 1992. New age determination of central Colorado Plateau laccoliths, Utah: Recognizing disturbed K-Ar systematics and re-evaluating tectonomagmatic relationships. Geological Society of America Bulletin 104 (12), 1547–1560.

Neves, S.P., Araújo, A.M.B., Correia, P.B., Mariano, G., 2003. Magnetic fabrics in the Cabanas Granite (NE Brazil): interplay between emplacement and regional fabrics in a dextral transpressive regime. Journal of Structural Geology 25, 441–453.

Olsen, P., Christensen, U., 1986. Solitary wave propagation in a fluid conduit within a viscous matrix. Journal of Geophysical Research 91 (B6), 6367–6374.

Paquette, J.-L., Ménot, R.-P., Pin, C., Orsini, J.-B., 2003. Episodic and short-lived granitic pulses in a post-collisional setting: evidence from precise U–Pb zircon dating through a crustal cross-section in Corsica. Chemical Geology 198, 1–20.

Peacock, S.M., 1990. Numerical simulation of regional and contact metamorphism using the Macintosh microcomputer. Journal of Geological Education 38, 132–137.

Petford, N., Kerr, R.C., Lister, J.R., 1993. Dike transport of granitoid magmas. Geology 21, 845–848.

Petford, N., Gallagher, K., 2001. Partial melting of mafic (amphibolitic) lower crust by periodic influx of basaltic magma. Earth and Planetary Science Letters 193, 483–499.

Pollard, D.D., Johnson, A.M., 1973. Mechanics of growth of some laccolithic intrusions in the Henry Mountains, Utah, II. Tectonophysics 18, 311–354.

Pritchard, M.E., Simons, M., 2002. A satellite geodetic survey of large-scale deformation of volcanic centres in the central Andes. Nature 418, 167–171.

Rabinowicz, M., Genthon, P., Ceuleneer, G., Hillairet, M., 2001. Compaction in a mantle mush with high melt concentrations and the generation of magma chambers. Earth and Planetary Science Letters 188, 313–328.

Rochette, P., 1987. Magnetic susceptibility of the rock matrix related to magnetic fabrics. Journal of Structural Geology 9, 1015–1020.

Rochette, P., Jackson, M., Aubourg, C., 1992. Rock magnetism and the interpretation of anisotropy of magnetic susceptibility. Reviews of Geophysics 30, 209–226.

Rutherford, M.J., Hill, P.M., 1993. Magma ascent rates from amphibole breakdown: an experimental study applied to the 1980–1986 Mount St. Helens eruption. Journal of Geophysical Research 98, 19667–19685.

Saint-Blanquat, M. (de), Tikoff, B., 1997. Development of magmatic to solid-state foliations during syn-tectonic emplacement of the Mono Creek granite, Sierra Nevada batholith. In: Bouchez, J.L., Hutton, D.H.W., Stephens, W.E. (Eds.), Granite: From Segregation of Melt to Emplacement Fabrics, pp. 231–255.

Saint-Blanquat, M. (de), Tikoff, B., Teyssier, C., Vigneresse, J.L., 1998. Transpressional kinematics and magmatic arcs. In: Holdsworth, R.E., Strachan, R.A., Dewey, J.F. (Eds.), "Continental transpressional and transtensional tectonics". Geological Society, London, Special Publications, vol. 135, pp. 327–340.

Saint-Blanquat, M. (de), Law, R.D., Bouchez, J.L., Morgan, S., 2001. Internal structure and emplacement of the Papoose Flat pluton: an integrated structural, petrographic and magnetic susceptibility study. Geological Society of America Bulletin 113 (8), 976–995.

Shaw, H.R., 1985. Links between magma–tectonic rate balances, plutonism, and volcanism. Journal of Geophysical Research 90 (B13), 11,275–11,288.

Stacey, F.D., 1960. Magnetic anisotropy of igneous rocks. Journal of Geophysical Research 65, 2429–2442.

Sullivan K.R., Kowallis B.J., Mehnert H.H., 1991. Isotopic ages of igneous intrusions in southeastern Utah: evidence for a mid-Cenozoic Reno–San Juan magmatic zone. Brigham Young University Geology Studies, 37, 139–144.

Thompson, G.A., Zoback, M.L., 1979. Regional geophysics of the Colorado Plateau. Tectonophysics 61, 149–181.

Tikoff, B., de Saint-Blanquat, M., Teyssier, C., 1999. Translation and the resolution of the pluton space problem. Journal of Structural Geology 21, 1109–1118.

Trindade, R.I.F., Raposo, M.I., Ernesto, M., Siqueira, R., 1999. Magnetic susceptibility and partial anhysteretic remanence anisotropies in the magnetite-bearing granite pluton of Tourao, NE Brazil. Tectonophysics 314, 443–468.

Trindade, R.I.F., Bouchez, J.L., Bolle, O., Nedelec, A., Peschler, A., Poitrasson, F., 2001. Secondary fabrics revealed by remanence anisotropy: methodological study and examples from plutonic rocks. Geophysical Journal International 147 (2), 310–318.

Uyeda, S., Fuller, M.D., Belshe, J.C., Girdler, R.W., 1963. Anisotropy of magnetic susceptibility of rocks and minerals. Journal of Geophysical Research 68, 279–291.

Webber, K.L., Simmons, W.B., Falster, A.U., Foord, E.E., 1999. Cooling rates and crystallization dynamics of shallow level pegmatite–aplite dikes, San Diego County, California. American Mineralogist 84, 708–717.

Zenzri, H., Keer, L.M., 2001. Mechanical analyses of the emplacement of laccoliths and lopoliths. Journal of Geophysical Research 106 (13), 781–792.